Department of Mathematics and Computer Science
Institute of Bioinformatics

Masters Thesis

Molecular Dynamics Simulations: What is the Effect of a Spin Probe on the Drug Loading of a Nanocarrier?

Marthe Solleder
Matriculation number: 4449223

Supervisors: Dr. Marcus Weber, Zuse Institute Berlin
Prof. Dr. Susanna Röblitz, Freie Universität Berlin

Submitted: March 14, 2016

Abstract

In this study a nanoparticle that is used for drug delivery is investigated. The main components under investigation are a dendritic core-multishell nanoparticle and a drug that will be loaded into the carrier. The loaded drug is dexamethasone, a steroid structure, and will be complexed in two variations with the polymer: the first complex consists of the unaltered dexamethasone structure whereas the second comprises of dexamethasone with an attached spin probe. The underlying research for this study is the following: a spin probe is attached to the structure to perform an electron spin resonance (ESR) spectroscopy, carried out to determine whether the loading of the drug was successful and at which position inside the carrier it can be found. It is presumed that the spin probe might influence the drug's behavior during loading and inside the carrier. This study is performed to investigate differences in the behavior of the two systems. The method of molecular dynamics simulations is applied on the two complexes, as well as free energy calculations and estimation of binding affinity, to determine if the attached spin probe is affecting the drug loading of the nanocarrier.

Acknowledgment

I would like to give my sincere gratitude to everyone who supported me during my master thesis. Special thanks go to my supervisors Marcus Weber and Susanna Röblitz as well as to my colleagues at ZIB, for their guidance and all their time spent on discussing any problems I faced. Furthermore, I am very grateful to my family and friends, especially my mother, for giving me the support and encouragements I needed throughout the last months.

Eidesstattliche Erklärung

Hiermit erkläre ich gegenüber der Freien Universität Berlin, dass ich die vorliegende Masterarbeit selbstständig und ohne Benutzung anderer als der angegebenen Quellen und Hilfsmittel angefertigt habe. Alle Ausführungen, die wörtlich oder inhaltlich aus anderen Schriften entnommen sind, habe ich als solche kenntlich gemacht. Diese Arbeit wurde in gleicher oder ähnlicher Form noch bei keiner anderen Universität als Prüfungsleistung eingereicht und ist auch noch nicht veröffentlicht.

Berlin, den 14. März 2016

Marthe Solleder

Table of Contents

Chapter 1

Introduction

1.1 Nanotechnology

The translation of the Greek word „nano“ is dwarf. In the International System for physical units nano corresponds to sizes of 10^{-9}m. The term nanotechnology therefore defines the technology dealing with matter of small size scales, such as atoms, molecules or supramolecules, and can be described as the „engineering of functional systems at the molecular scale“ [1]. The US American government program National Nanotechnology Initiative [2] published the following definition: „Nanotechnology is the comprehension and observation of particles with sizes of one to 100 nanometers“. Others, as has been outlined by G. Schmid [3] for instance, refer nanotechnology not only to the aspect of scale. Brune et al. [4] give the following definition excluding any specific size reference: „Nanoscience deals with functional systems, either based on the use of subunits with specific size-dependent properties or of individual or combined functional subunits“. Here it becomes clear that the important and defining aspects of nanotechnology are unusual and innovative properties of nanomaterials. Such properties are not bound to particles of sizes between one to 100 nm, but can be observed below and above this given range, too. Thus, any restriction to an absolute size definition would be incongruous and limit possible novelties of nanotechnology. Nevertheless, newly discovered and developed so-called nano-effects mostly arise with materials on the above defined nanoscale, such that the first definition gives a reasonable interpretation for the term „nanotechnology“. Figure 1.1 shows the size range from 0.1 to 100000000 (10^8) nm with correspodning (bio-)molecules. From sizes 1 to 100 nm, several nanomaterials, that are common in the various areas of nanotechnology, are presented to outline their sizes compared to other biological and chemical structures.

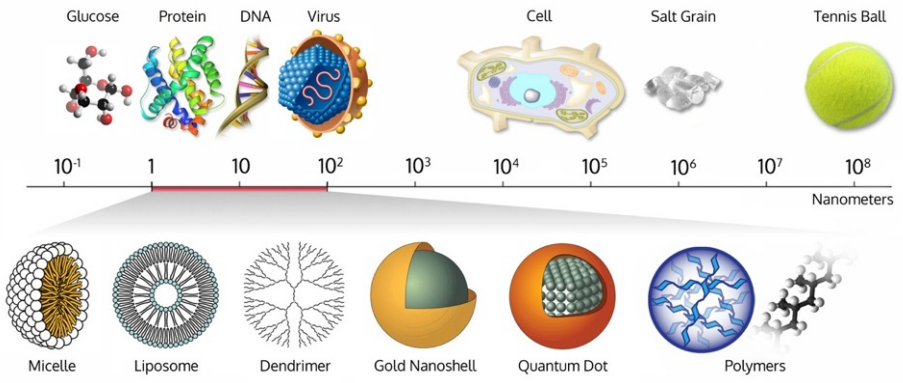

Figure 1.1: Size presentation of divers molecules, including nanomaterials in the range of 1 to 100 nm (Source: WICHLab, Johannes Gutenberg-Universität Mainz [5]).

Chemical substances can show completely new chemical properties when available at nanoscale or at a different size compared to its original existence. This feature was adopted in research on nanotechnology to receive novel substances with new characteristics or to strengthen known properties of similar structures. For decreasing particle size, hence for particles downsized to a nanoparticle, the number of surface molecules of the particles increases [6]. This effect can be seen in Figure 1.1 for instance: micelles, consisting of one lipid layer and presenting all of its particles on the surface, have a smaller size as liposomes. Liposomes consists of both, particles defining the surface and particles excluded from the surface. This high percentage of surface molecules can lead to particles with novel characteristics such as higher chemical reactivity, strength, heat resistance, or electric conductivity, compared to bigger particles of the same substances. This capability of transforming materials and structures in a way that enable the development of novel properties simultaneously causes drawbacks. These new developed structures can entail the risk of a higher toxicity with so far mostly undetected impacts on humans and the environment. Therefore, for every new discovered material with profitable characteristics, studies have to be performed to detect and eliminate risks and hazards.

Applications With increasing possibilities and discoveries in this research discipline, nanotechnology is nowadays applied in many different areas. In electronics for instance, nanotechnology is used to develop materials providing novel properties to improve displays or power consumption of electronic devices. Nanotechnology is also applied in the field of solar technology by decreasing the manufacturing costs of nanotech solar cells compared to traditional solar cells. Additionally, nanotech-

nology can be applied to technologies of cleaning water. Industrial waste can be removed by nanoparticles that induce a chemical reaction of the contaminating chemicals to make them non-hazardous. In the fashion and textile industry, nanotubes have been developed to produce stain-resistant textiles as well as fabrics with other novel property, retaining weight, thickness or stiffness of conventional fabric. Furthermore, nanotechnology is applied in developing novelties in food science, such as allowing new ways of food packaging for better conserving its content. With nanotechnology new methods are established to induce higher levels of nutrients and vitamins in food and to benefit simultaneously of controlled transport and release of these nutritious substances after intake.

Medicine is another important field of nanotechnology application. Nanoparticles are used as diagnostic techniques like monitoring the nitric oxide level in the bloodstream or in drug development. For the latter, nanoparticles serve as nanocarriers, meaning that a drug can be loaded into such a nano structure. The resulting complex is then jointly transported into the organism and, more important, carried to its effect-specific area. By this, drug delivery treatment can be improved and targeted to leave uninfected, healthy regions of the body undamaged. The therapeutic effect is influenced tremendously by location and amount of drug release and often a certain concentration of drug needs to be obtained for a successful treatment. Conventional treatment is characterized by a high initial drug concentration in the organism and a subsequently rapid decrease, quickly falling below the therapeutic range of concentration [3, Chapter 2.2.4]. New methods for sustained-release of drug are developed resulting in medicine providing a longer time period of drug release at a constant level. Those techniques are based on the concept of host-guest systems and use interactions like hydrogen or van der Waals bonds and electrostatic interactions [3, Chapter 2.2.4], by which the speed of drug release is adjusted for the corresponding treatment. In the development of cancer treatments the implementation of this method is aspired to deliver chemotherapy drugs only to cancerous cells. Superparamagnetic iron oxide nanoparticles are an example for such a drug delivery system [3, Chapter 2.2.4]. They are applied to deliver drugs into tumor tissue and are transported into the corresponding areas by external high-gradient magnetic fields. Drug release can then be triggered by several effects such as change of temperature, pH-value or even enzymatic activity [3]. Superparamagnetic iron oxide nanoparticles are also used in gene therapy. With DNA sequences bound to their surface, those nanoparticles can enter cells with the use of receptor-mediated endocytosis. Once the particle reached the intracellular space, the DNA can emerge from the particle's surface and invade the nucleus – a so-called non-viral transfection is performed. Furthermore, silver nanoparticles are known to show many useful properties in medical use. They have an effect as

antibacterial agents, they act anti-fungal, anti-viral and anti-inflammatory, which made them useful for multiple drugs, for instance also as chemotherapeutics.

First research about nanotechnology was recorded in the middle of the 20th century and over time it received more and more interest and attention from different sectors. By early 2000, nanotechnology was of high interest in many areas of research, politics, and commercial, but not only because of innovative development but also due to disagreement about the number of benefit and risk. Just looking at the development and amount of innovations of the last years and the speed with which the evolution took place, one can only imagine what and how much more can be developed in the future in the field of nanotechnology.

1.2 MD Simulation

In the past years, besides existing techniques to perform experimental research, a new method, called the in silico method, was developed and gained more and more popularity and credibility in many different fields of research. With the use of computational calculations, properties of systems and processes can be established leading to reliable results. Before the discovery of computers and computer simulations, scientific research consisted of theoretical and experimental research. Properties of a molecular system could therefore only be predicted by applying theory that approximately described the underlying molecule. Examples of such approximation methods for material properties are the van der Waals equation for dense gases or the Boltzmann equation for properties of transport of dilute gases. Computer simulations can test a theory before it is performed experimentally as well as help to design real world experiments. Through increasing research activities with computer simulations, the importance of computer experiments was established: some long-accepted theories had to be revised and enhanced the possibility of constructing new theories, as nowadays a study is often divided into a primary computer experiment followed by real world experiment, into which alterations and improvements detected in the previous computer simulation can be included.

The first records of a performed molecular dynamics simulation date back to 1959 [7]. Since then, a lot has been changed concerning the methodology of computer simulations, but the basic idea remained the same in today's algorithms and tools applied to recent research. An advantage of performing computer simulations on a molecular system is that experimental settings that would be difficult to perform and maintain in real life experiments are feasible in computers experiments, mean-

ing that properties of molecules and materials can be predicted easier and often cheaper. Furthermore, in the development of new materials, computer simulations can be used to study them and predict properties and characteristic without those new materials even being physical available yet. Other applications of molecular dynamics simulations are to investigate physical properties and movements of atoms or even particles. Molecular dynamics' application range from various researches of disease patterns and causes to studies of drug effect mechanisms and drug design.

The basic idea behind a molecular dynamics algorithm is to create a time evolution of the system of interest by computing the development of several properties for a sufficiently long time and by that estimate an average behavior of the system. Molecular modeling, the technique of imitating the molecular behavior for the purpose of analyzing particles or whole systems, has already been performed for many years, but with increasing computational techniques it was revolutionized and developed for usage in a much wider range.

1.3 Electron spin resonance (ESR) spectroscopy

Electron spin resonance (ESR) spectroscopy, also known as electron paramagnetic resonance (EPR) spectroscopy, is a spectroscopic technique to investigate material properties by looking at interactions between matter and electromagnetic radiation. To perform an ESR/EPR spectroscopy, a molecule or ion under investigation has to be paramagnetic which is fulfilled when the particle includes one or more unpaired electrons. Structure and spacial distribution of paramagnetic species can be detected with the ESR/EPR spectroscopy by detecting signals from excited electron spins that are interacting with a magnetic field. Application of ESR/EPR spectroscopy is in particular used in studies of metal materials or organic radicals. Increasing progress in the field of ESR/EPR spectroscopy made it possible to use it also for structural analysis of biological systems. With site-directed spin labeling into proteins or other cell biological elements for instance, ESR/EPR spectroscopy provided new ways to identify physical and chemical properties of the underlying molecule [8]. This means, that a studied structure does not necessarily need to be paramagnetic itself but can achieve paramagnetic characteristics by attaching a so-called spin probe with the relevant properties. A specific application of EPR spectroscopy with attached spin markers is the field of polymer science: with this method a polymer can be understood, designed or manipulated on a molecular level [9].

There exist different kind of attachable spin markers such as nitroxide radicals,

which are used in most of EPR sepctroscopic experiments on systems being diamagnetic by nature. An example of a nitroxide spin marker is shown in Figure 1.2(a), the so-called TEMPO nitroxide radical, of which many applicable derivatives exist [9]. Also belonging to the class of widely used nitroxide radicals is the group of five ring analogs of the TEMPO marker, such as the PROXYL spin probe depicted in Figure 1.2(b).

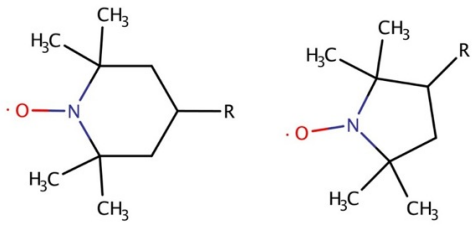

(a) (b)

Figure 1.2: Nitroxide spin marker TEMPO (a) and five ring analog PROXYL (b) [9].

Study The following study investigates a nanocarrier used in the development of dermal drug deliver treatment. For the development of a novel medication using nanotechnology, it is crucial to be certain that the drug was actually captured inside the nanocarrier during synthesis. Furthermore, it is relevant to know where inside a specific nanocarrier the drug is favorably positioned. Also, the kind of nanotransporter should be chosen depending on the properties of the delivered drug as well as the environment and time the drug should be released from the carrier. Nanocarriers are often synthesized using emulsion techniques but those carriers have been detected to present a low drug loading and drug encapsulation rate which made them unprofitable to use in drug delivery [10]. To examine if the drug was loaded successfully into the carrier, an electron spin resonance spectroscopy can be performed. Prior to the spectroscopy, a spin probe is attached to the drug. This spin marker naturally changes the properties of the drug. On the one hand, changing the properties (providing the structure with an unpaired electron) is required to receive a signal in the performed ESR spectroscopy but on the other hand it might influence the behavior of the original drug strongly. Essential questions arise whether attaching a marker to obtain a result actually biases the result in the first place: Does a drug behave differently inside a nanocarrier if it is extended by a spin probe? Is ESR spectroscopy a good way to use as prediction for drug loading?

In general, molecular dynamics simulations are used to predict the behavior of a given system for a certain period of time. Here in this study, molecular dynamics calculations are performed to investigate the drug and its spin marker attached analog, and whether they unveil a different behavior when inside the nanocarrier or not.

Aim of this study is to give assumptions about a specific nanocarrier-drug-complex to be used in the treatment against skin diseases. Topical treatments often show difficulties to be absorbed as only a few percent of the drug have an effect due to high concentrated drug release in a restricted, short period of time. As this is often not sufficient to treat a disease, higher doses or systemic treatments using oral medication are necessary. By this, the possibility of side effects are increased, as well as higher costs and, depending on the prescribed drug and the frequency of medication intake, a decrease of the effect of the compound. Therefore, in many areas of drug development, local and controlled drug released is a desired effect which can improve the healing process as well as the chances of recovery and cure.

Chapter 2

Materials

2.1 Molecules of the System

The system under investigation in this research consisted of a nanocarrier and a drug that was inserted into the carrier, the subsequently presented dexamethasone. Molecular Dynamics calculations were performed on the system to examine its behavior over a certain period of time and to evaluate binding affinities. At first, the system's components were built and processed separately.

Dexamethasone Dexamethasone belongs to the group of steroid drugs used to treat inflammation. Endogenous steroid structures are for example lipid cholesterol, estradiol, and testosterone. One famous representative of steroid hormones is also known as cortisone or corticosteroids which realizes diverse biological function within an organism, such as appearing as a signaling compound or activating steroid specific receptors. Furthermore, some steroids function as important building blocks within cell membranes. Drugs based on structural characteristics of steroids intervene with the immune system by suppressing immune response as well as fighting histamines, that were released in an allergic reaction. The chemical formula of the steroid drug dexamethasone is $C_{22}H_{29}FO_5$ and it has a molecular mass of 392.461 g/mol. The chemical structure is shown in Figure 2.1. It consists of three cyclohexane and one cyclopentane rings, as is a property of all steroid structures. To this structure of four rings, different functional groups can be attached defining the various steroids with their differing functions and characteristics. Dexamethasone, has an anti-inflammatory effect and is prescribed to patients with Chron Disease, it is used in the therapy of rheumatic patients, as well as jointly with other medication given for the treatment of some cancers. Furthermore, dexamethasone is used to treat skin diseases. Depending on the treatment, dexamethasone can be administered as an oral treatment, as an injection or as an

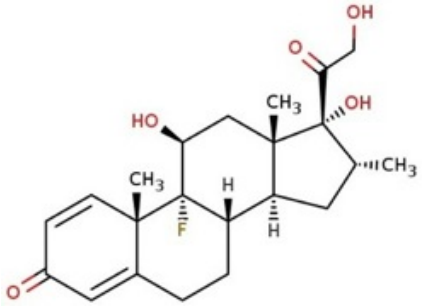

Figure 2.1: Chemical structure of dexamethasone.

ointment. Dexamethasone is synthesized in the following steps: initial structure is 16β-methylprednisolone acetate. With dehydration it is transformed into the 9,11-dehydro derivative and afterwards exposed to a hypobromite (HOBr) source and converted into a 9α-bromo-11β-hydrin derivative. Sodium hydroxide (NaOH) and hydrogen fluoride (HF) perform the final conversions into dexamethasone.

As a second structure, a variation of this drug is used in this study. Dexamethasone was expanded with a spin probe attached to the terminal hydroxy group of the functional group. The spin marker used in this study is PROXYL, a five ring analog of the nitroxide radical, that was depicted in Figure 1.2(b) of Chapter 1.3. The chemical structure of dexamethasone including the attached spin marker is presented in Figure 2.2. Those two ligand structures were built with the chemical

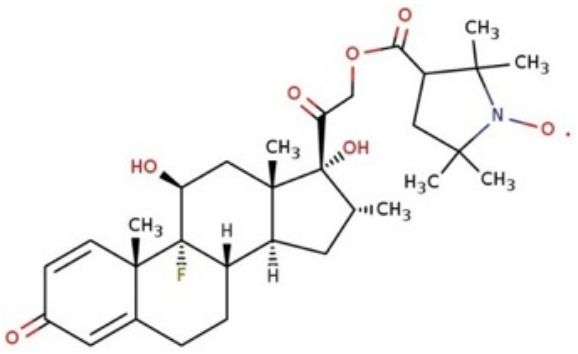

Figure 2.2: Chemical structure of dexamethasone with attached spin probe.

drawing software MarvinSketch [11], extracted as Cartesian coordinate files and could be used as input structures for the subsequent preparatory steps performed prior to the molecular dynamics calculation.

Polyglycerol Nanocarriers are particles that can transport smaller molecules from one place to another (cf. Chapter 1.1). There are many different types of commonly used nanocarriers such as micelles, liposomes or polymers. The material characteristics of such carriers allow the transport of drugs with different properties, such as hydrophobicity or hydrophilicity, to a specific area inside the body. The nanocarrier used in this study consists of a polyglycerol amine core with an double-layered outer shell made of a C_{18}-alkyl chain (lipophilic) and monomethoxy polyethylene glycerol (mPEG, hydrophilic). These appending branches of the outer shell serve as the framework embracing the loaded drug and are defined together with the polyglycerol core as a core multishell nanotransporter (see Figure 2.3). Especially the lipophilic and hydrophilic properties of the outer shell enable CMS nanocarriers to transport different kind of drugs to polar but also nonpolar regions [12]. This lipophilic characteristic of the CMS nanotransporter makes the carrier also usable in the development of topically administered ointments. Topical treatment furthermore benefits from the reduced risk of side affects [12].

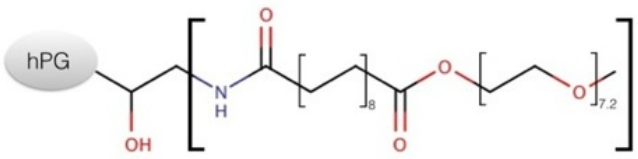

Figure 2.3: Chemical structure of the core multishell nanotransporter.

These polyglycerol structures, that consist of repetitively linked subunits are called dendrimers. Dendrimers have a highly branched core forming the three-dimensional structure and branches of the outside shell provide the structure with varying characteristics. See Figure 2.4 for a graphical representation of the gradual construction of a dendrimer with several intermediate steps of increasing sizes. An algorithm to assemble a polymer structure out of individual glycerol monomer building blocks was introduced by V. Durmaz in [13].

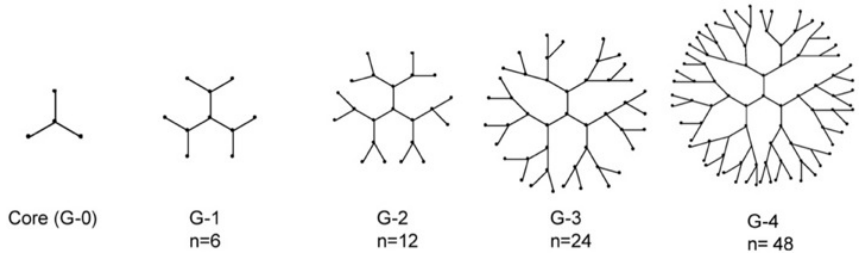

Figure 2.4: Dendrimer constructions of various sizes (Source: [14]).

Polymer Building Algorithm In [13], V. Durmaz had developed an algorithm to automatically assemble monomer building units to a large structure and form the polyglycerol, as large as required for a subsequent research. Initially, parameters defining construction order, branching type and polymer size need to be defined. The constructed polymer can be seen as an acyclic graph $G(V, E)$, with $|V|$ being the number of monomers in the polymer and $|E|$ denoting the bonds between monomers. A bond between two building units is formed between an oxygen atom of the predecessor, which is a deprotonated hydroxy group, and dehydroxylated carbon atom of the successor monomer [13]. In Figure 2.5(b), different polyglycerol building introduced by V. Durmaz for the polymer assembly units are shown, all derived from the original glycerol monomer (Figure 2.5(a)). These five

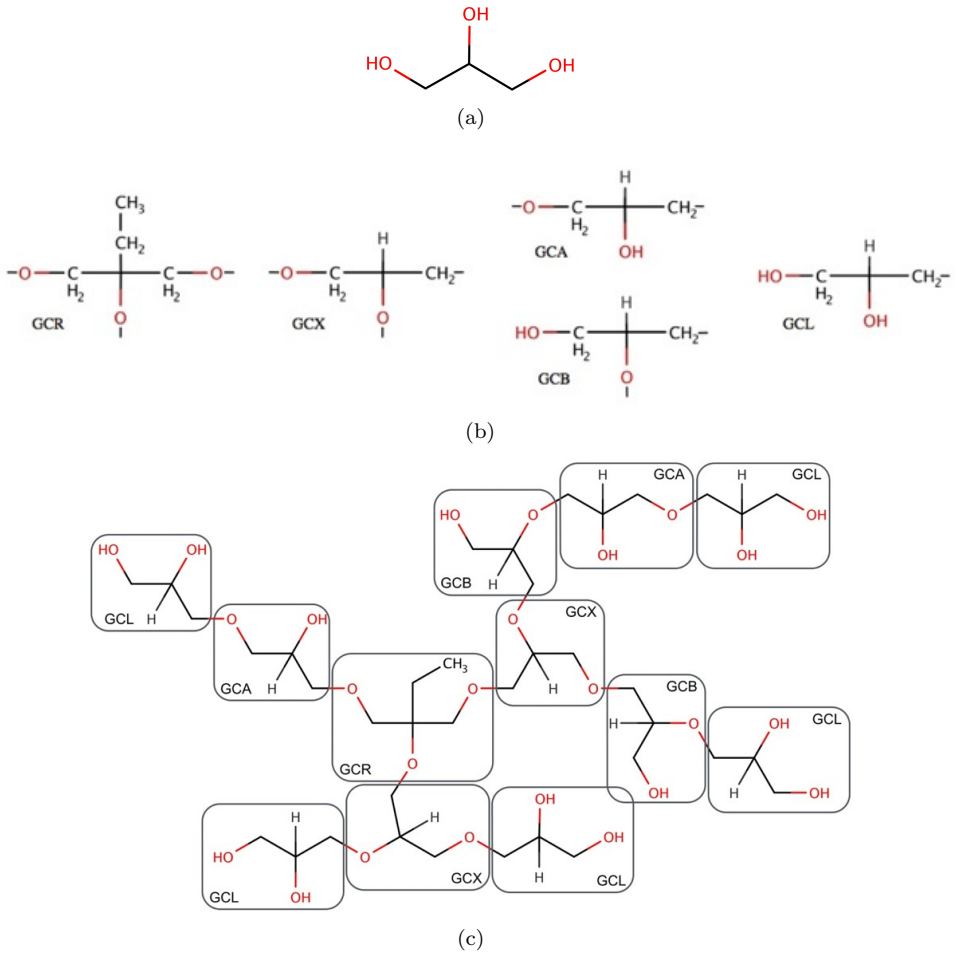

Figure 2.5: Glycerol monomer (a), building units (b) and a small example of a constructed polyglycerol (c) (depicted according to [13]).

different kind of monomer units each perform a different task in the assembly of a polyglycerol structure. There exist one root and one leaf element, GCR and GCL, and three centerpieces. Two of them can be linked twice, the linear GCA and GCB units, and the third is a trivalent branching block, GCX. The amount of missing hydroxy hydrogen atoms in a unit $i \in V$ corresponds to the number of successor monomers this particular unit has, meaning the outdegree n_i^s of the unit. Respectively, the amount of hydroxy groups a unit $i \in V$ is missing equals to the unit's predecessors, thus the indegree n_i^p of the unit. The total amount of connections v of a building unit i can be described by $v = n_i^s + n_i^p$ (the connectivity of a unit, [13]). The different units have varying connectivity, since they vary in their position within a polyglycerol. The root element GCR for instance has no predecessor but three successors, whereto the leaf unit GCL completes a branch of the polyglycerol and therefore has only one predecessor and no successor (see table 2.1 for detailed information).

$i \in$ GC*	n_i^s	n_i^p	
GCR	3	0	unique source of the graph
GCX	2	1	branching monomer
GCA/GCB	1	1	linear monomer
GCL	0	1	terminal monomer (leaf)

Table 2.1: In- and outdegree of polyglycerol building units [13].

The total number of terminal units n_{GCL} can be established from the number of monomers used so far. Only monomers are taken into account that have a total amount of three absent hydroxy hydrogens or hydroxy groups (GCR, GCX):

$$n_{\mathrm{GCL}} = \sum_i (n_i^s - n_i^p) \cdot n_i, \text{ with } i \in \{\mathrm{GCR}, \mathrm{GCX}\} \tag{2.1}$$

[13]. After having started with one root monomer GCR, the algorithm adds branching and linear monomers to the structure and simultaneously develops a list with the number of open binding sites that need to be concluded with a leaf unit in the end. This is done to keep track of the overall number of monomer units and to secure that the overall amount of monomers does not exceed the initially defined value. The addition of one of the linear units to the increasing polyglycerol structure does not change the number of subsequently added leaf unit since its indegree and outdegree compensate each other: $n_i^s + n_i^p = 0$ for $i \in \{\mathrm{GCA}, \mathrm{GCB}\}$. Once the size of the current polyglycerol and the amount of open binding sites sum up to the initially specified number of assembled monomers, the algorithms stops the development of the polyglycerol and completes the branches by attaching leaf units. An example of a small polyglycerol, constructed with the algorithm is shown in figure 2.5(c).

Additional Polyglycerol Building Unit In this study, a new monomer for the polymer structure is introduced: to provide longer terminal branches of the polyglycerol an additional leaf unit had to be included in the algorithm. First of all, the structure of the additional polyglycerol component is drawn and exported into a Cartesian coordinate file using again the chemical editor MarvinSketch [11] (see Figure 2.6). This structure is then parameterized according to the *amber99sb* force field [15] with the Python based tool *acpype* using Antechamber [16]. Antechamber, a class of programs widely used in molecular mechanic studies, can recognize atom types within the coordinate files, it produces topology files of the residues and, if some force field parameters are missing, it compensates them with the most similar and most suitable replacements. The output of the parameterization step provides both, a new Cartesian coordinate file as well as topology files including further data of the structure, which are used by the algorithm as basic structure for the polyglycerol assembly. To ensure an uncharged structure of the unit, *acpype* parameterization was conducted including the hydrogen atoms. After parameterization, hydrogens were removed from the new coordinate file with the toolkit open babel [17, 18], to match the data used in [13]. The above presented algorithm of V. Durmaz [13] was expanded with the new building block GCT to build a new hyperbranched polyglycerol. The constructed core multishell nanotransporter consisted of 150 single building units and had an overall diameter of 11 nm. Figure 2.7 displays a 3D representation of the nanocarrier structure constructed for this study consisting of the polyglycerol core (yellow) and the outer shell made of GCL and GCT (red). One main requirement to the construction of the polyglycerol in this study was the ratio between the two leaf units forming the outer shell of the carrier. The outer shell was characterized to have a proportion of 70 % new introduced GCT units and 30% usual glycerol monomers units (GCL).

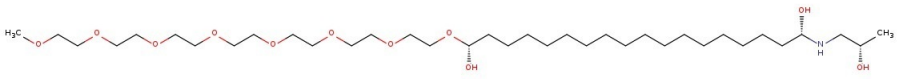

Figure 2.6: New glycerol monomer building unit.

2.2 Force Field

Well-known and frequently used classical force fields besides the AMBER class, to which *amber99sb* belongs, are the CHARMM force field (developed for macromolecules) and the GROMOS force field (part of the molecular dynamics computer simulation package GROMOS for biomolecules). Furthermore, there exist other groups of force fields, such as polarizable force fields for dealing with the influence

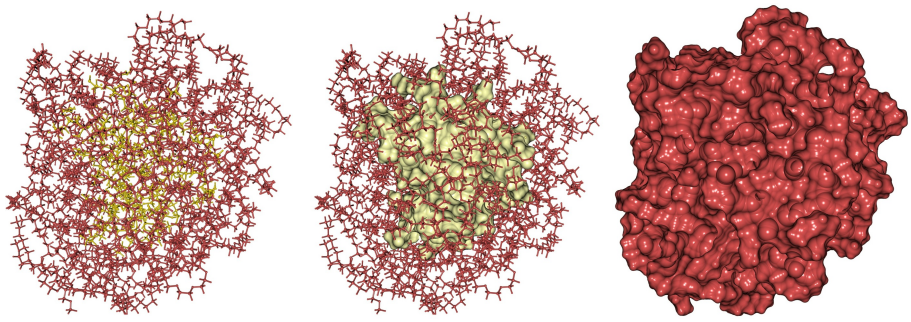

(a) (b) (c)

Figure 2.7: New polyglycerol structure, presented with only molecular structure (a), with molecular structure and the core as molecular surface (b) and as a whole molecular surface representation (c). The core structure (yellow) is surrounded entirely by the outer shell (red).

of the environment to the molecule's charge, reactive force fields, used for constant bond formation and breaking, and coarse-grained force fields that are utilized when simulating larger molecules, providing a reduction of computational costs.

A force field can be described as a function that computes the potential energy of a particle by using defined parameters characterizing the utilized atoms. Force fields of molecular modeling are empirical, meaning that there does not exist the one correct set of parameters for any molecule but more an approximation of a good description for a specific set of atoms with its characteristics and properties. There exist different kind of force fields, often grouped into classes of force fields, which are usually specific to use for a certain group of molecules. It can be differentiated between force fields that have been designed to just study one atomic or molecular species, a whole class of molecules or even a large range of molecule classes. This means, that force fields are transferable, since one set of parameters can be used on many different but related structures. One example is the class of AMBER force fields from AmberTools [15], which was used in this study. AMBER force fields are known to work well with proteins and nucleic acids. Looking at the mathematical aspect, the „best choice“ of a force field for a molecule means the ability to calculate the first and second derivative of the energy of this specific set of atoms with respect to its coordinates. This is necessary for the computation of the energy minimum as well as the calculation of molecular dynamics. This will be outlined in more detail in Sections 3.2 and 3.3. Often a force field that has the most precise functional form for a given molecule may be inadequate concerning the computational costs, therefore the choice of the best force field has to be a compromise between precision and efficiency. But with today's increasing compu-

tational performances, it is more and more possible to apply the most accurate functional force field to a system.

Atoms of a structure interact with each other in various ways. They can show bonded or non-bonded interactions. Thus, direct bonds between two atoms, angles of three successively ordered atoms, connected with two bonds, and bond rotation of four consecutively bound atoms need to be defined as well as non-bonded interaction concerning electrostatic and van der Waals forces (see Figure 2.2). How well a force field is applicable to a system is often conditional to just a small number of certain parameters, such as non-bonded and torsional terms (parameters for the soft degree of freedom) [19]. The terms of bond-stretching and angle-bending (parameters for the hard degrees of freedom) on the other hand do not belong to the group of sensitive parameters, since those values do not affect simulation results considerably. In general, parameters of a force field need to be looked at as an entity and they can not be simply transferred individually from one force field to the other. But, the force field's hard degrees of freedom are more robust and independent and can therefore be transferred to another force field without further ado, whereto parameters of the soft degree of freedom are connected closely and influence each other [19].
Electrostatic forces capture the interaction of electrically charged particles and van der Waals forces describe the potential of all other, not covalently bound atomic or molecular interactions. Each of the just described terms defined in a force field

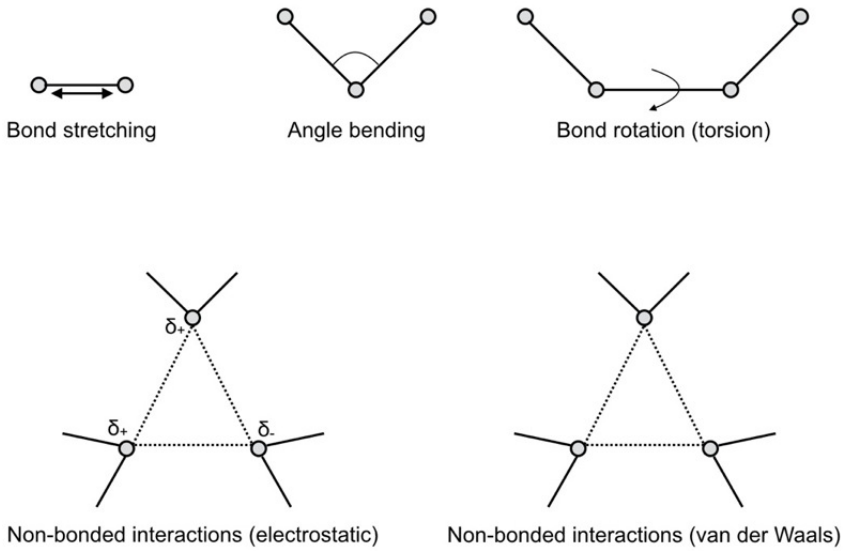

Figure 2.8: Atomic binding characteristics for a force fields (depicted according to [19, Figure 4.3, Chapter 4.1.1]).

(outlined in Figure 2.2) contribute differently to the potential energy of the system. In a very rough and simplified way, the potential energy $\mathcal{V}$ can be defined by the following:

$$\mathcal{V}_{total} = [\mathcal{V}_{\text{bonds}}] + [\mathcal{V}_{\text{angles}}] + [\mathcal{V}_{\text{torsions}}] + [\mathcal{V}_{\text{non-bonded interactions}}] \tag{2.2}$$

[19, chapter 4.1]. The potential energy is calculated as a sum of the single terms for the bonded, angle, torsion and non-bonded interaction of a particle. In a more detailed description, Equation 2.2 can be transformed into

$$\begin{aligned}\mathcal{V}(r^N) = &\sum_{\text{bonds}} \frac{k_i}{2}(l_i - l_{i,0})^2 + \sum_{\text{angles}} \frac{k_i}{2}(\theta_i - \theta_{i,0})^2 + \sum_{\text{torsions}} \frac{V_n}{2}(1 + \cos(n\omega - \gamma)) \\ &+ \sum_{i=1}^{N} \sum_{j=i+1}^{N} \left(4\epsilon_{ij} \left[\left(\frac{\sigma_{ij}}{r_{ij}} \right)^{12} - \left(\frac{\sigma_{ij}}{r_{ij}} \right)^{6} \right] + \frac{q_i q_j}{4\pi\epsilon_0 r_{ij}} \right)\end{aligned} \tag{2.3}$$

with the potential energy $\mathcal{V}$ being a function of the positions r of N particles, mostly atoms [19, chapter 4.1]. The first expression in Equation 2.3 describes the interaction of bonded atoms by using a harmonic potential of the energy that increases if bond length l_i differ from $l_{i,0}$, a reference bond length. Secondly, all angles of the molecule are summed up, also with the use of a harmonic potential and with θ denoting the angles between any two atoms. How the energy changes when a rotation between bonds occurred (described by two angles ω and γ) is captured in the third term. Non-bonded interactions, described in the last term of Equation 2.3, are computed between every pair of atoms i, j, with i and j belonging to different molecules or to the same but with a distance of at least three bonds. Those interactions are often modeled with a Coulomb (electrostatic interactions) and a Lennard-Jones (van der Walls interactions) potential.

The definition of atom types is a crucial concept when preparing most molecular systems for computational simulations and is therefore included in most force fields similarly. Atomic numbers are specified, as well as the geometry of the system, the overall charge, and spin multiplicity. Furthermore, atom types in a force field indicate the hybridization state of an atom. A carbon atom for instance can be existing in different orbital hybridization states: atoms can be present in a tetrahedral arrangement (denoted as sp^3 hybridization), they can show a trigonal geometry (described as sp^2-hybridized) or be arranged linear (sp hybridization, see Figure 2.9 for details). Those properties are relevant when considering the angles θ_0 between the carbon atoms. For instance for the tetrahedral arrangement, θ_0 is defined as approximately 109.5° and for a trigonal order it is sset to 120°.

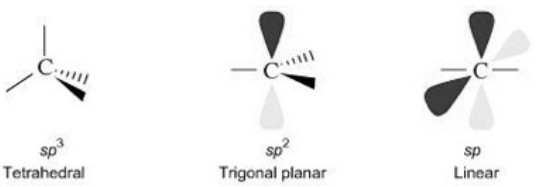

Figure 2.9: Orbital hybridization of a carbon atom (Source: [20]).

Force Field Extension For the performance of the molecular dynamics simulation in the course of his research [13], V. Durmaz included the polyglycerol building blocks into the *amber99sb* force field. Meaning that each of the polyglycerol components are force field known residues and all necessary information about bonds, angles, bond rotation, and non-bonded interactions of each of the units was available within the force field. This is mainly done to achieve a quicker parameterization of the big macromolecule consisting of a large amount of atoms. In the case of this study, the polymer consisted of 150 single building units that add up to 5793 atoms in total. Parameterization using the extended force field can be performed with a Gromacs tool [21, 22, 23, *pdb2gmx*] that is designed for big molecules such as proteins or DNA fragments. Other parameterization tools, such as *acpype* [16], can be applied to structures consisting of residues not included in the utilized force field but require much more computational time and cost. Therefore, the newly introduced polyglycerol monomer GCT also needed to be included within the library of the *amber99sb* force field. To expand a force field with a new structure, the overall residue name needs to be declared as well as all atoms and bonds within the structure have to be outlined. Furthermore, information about its hydrogen atoms needs to be deposited, since the polyglycerol building units are used without hydrogens, and every potential bond of this new unit to other force field included structures has to be indicated and described precisely.

When extending the force field with a new unit, its charge required special attention, too. As has been outlined by V. Durmaz [13], a neutral charge of the constructed polyglycerol is essential for the subsequent simulation, therefore partial charges c_i of all units $i \in \mathrm{GC}^*$ were altered to a fitted charge $\bar{c}_i$ to ensure zero overall charge. The missing hydroxy hydrogens and hydroxy groups belonging to a building block impact a unit's overall charges differently: removing a hydroxy group increases a unit's charge whereas the elimination of a hydrogen atom reduces it. The work of V. Durmaz [13] states that the leaf units possessed a (fitted) positive charge $\bar{c}_{\mathrm{GCL}} = \alpha$. The number of required leaf units GCL is composed by

the amount of added units that introduce a new branch within the polymer structure: the root monomer (GCR), being the core of the polymer, introduces three branches and thus requires three leaf units. Each thereto appended unit either keeps the total amount of necessary leaf units stable (GCA, GCB) or increases it by one through adding a branch (GCX). Therefore, these units need to compensate the positive charges of the terminal building blocks:

$$\bar{c}_{\mathrm{GCR}} = -3\bar{c}_{\mathrm{GCL}} = -3\alpha \tag{2.4}$$

and

$$\bar{c}_{\mathrm{GCX}} = -\bar{c}_{\mathrm{GCL}} = -\alpha \tag{2.5}$$

[13]. The fitted charge of GCL was estimated by

$$\alpha = \frac{\sum_i |c_i|}{\sum_i |n_i^p - n_i^s|} = 0.2177 \tag{2.6}$$

leading to

$$c_i = (n_i^p - n_i^s) \cdot \alpha \tag{2.7}$$

for each of the non-linear units [13]. The linear monomers GCA and GCB do not increase the amount of additional leaf monomer. Therefore they do not have to compensate a terminal unit's positive charge and were attributed with an overall zero charge:

$$c_{\mathrm{GCA}} = \bar{c}_{\mathrm{GCB}} = 0. \tag{2.8}$$

Since the new introduced building unit GCT replaced original leaf units GCL in some of the polyglycerol's branches, its charge corresponds to the charge of the original leaf structure. The charges of each atom j of the unit GCT, values received by the parameterization with *acpype*, were modified with

$$c_i(j) = c_i(j) + \frac{\bar{c}_i - c_i}{n_i},\ i = \{\mathrm{GCT}\} \tag{2.9}$$

[13]. These minor manual adjustments did not have a considerable impact on further steps and results, since there does not exist a correct partial charge of any atom. In this case, the charges of each atom of GCT had only been modified by 0.35 to 6.5 percent plus or minus the charge received from parameterization.

With this new unit included in the force field, the polyglycerol structure could be processed for subsequent preparatory steps and the MD calculations using the modified force field library *amber99sb*.

Chapter 3

Methods

The methods used to perform the computational experiments of this study, the molecular dynamics simulations, consisted of first preparatory steps of the data and subsequently executed MD calculations.

3.1 Parameterization

Parameterization is responsible to generate different files of the structures processed, that are needed for the subsequent computational steps. On the one hand, a topology file of the system is produced containing all information about bonds, angles, dihedrals, and charges of the atoms. Moreover, the parameterization produces a position restraint file that defines restrains on assigned groups of atoms. Another file resulting from the parameterization is a new coordinate file of the system that contains all input information of the structure but also possibly new data, since parameterization can detect missing information of a molecule using the force field, such as adding absent hydrogen atoms.

In this research, the parameterization of the polyglycerol was performed using Gromacs [21, 22, 23, *pdb2gmx*] applying the beforehand extended *amber99sb* force field [15]. The applied Gromacs tool requires several parameters and input data (see Appendix A.1 for details) and outputs the necessary files of the polyglycerol for the subsequent simulation.

The drug that is loaded into the polymer nanocarrier, dexamethasone, was parameterized with *acpype* [16], the same tool that was used for the preparation of the polymer units. But instead of applying also the *amber99sb* force field, as presented earlier, the general amber force field *GAFF* is used for dexamethasone. *GAFF* is a force field suitable for drug design and includes parameters for a wide

range of organic molecules consisting of the standard atom types. Moreover, the two force fields *amber99sb* and *GAFF* are compatible and therefore it is possible to use both of them within the same simulated system and applying each one depending on its suitability for the current step of the process and the processed structure.

After parameterizing the two structures separately, some further steps had to be conducted before starting the computational experiment. When calling the parameterization tool, the decision whether the simulation is performed in a solvent or within vacuum has to be made. Normally, to provide the most natural cell-like conditions to a simulated system, a solvent is added, usually water. When creating a new structure, like the polyglycerol carrier of this study, a vacuum simulation is needed to make sure the structure has at reasonable conformation and energy level before starting to analyze the data. Consequently, the polyglycerol was first simulated solely in vacuum. Using the output of the first simulation to extract an appropriate conformation of the polyglycerol, a second simulation round was performed, here denoted as „pull run“, including the ligand under investigation, dexamethasone. This run was carried out with a solvent (water), thus with the use of the Gromacs package [21, 22, 23] a simulation box was defined and solvent molecules as well as ions, compensating existing charges, were added. As a concluding preparation before initializing the molecular dynamics simulation, a final verification is performed: Gromacs checks for invalid content of the files, performs a translation from a molecular description to an atomic description and reads in parameters given in a parameter file for the subsequent simulation [21, 22, 23, *grompp*].

Following to the above mentioned preparation steps, which included the parameterization and the arrangement of a simulation environment, the molecular dynamics (MD) simulation is conducted, consisting of three individual calculations: an energy minimization (described in Section 3.2), followed by an equilibration (Section 3.3.1) and a concluding MD computation for actual data collection (presented in Section 3.3.2).

3.2 Energy Minimization

The energy minimization can be described as the search for the lowest energy state of the system. The term „energy“ means the potential energy of a system or a molecule and is a multidimensional function of the coordinates of the underlying system, a function of $3N$ Cartesian coordinates for a system of N atoms. A. Leach gives a formal definition of the energy minimization [19, Chapter 5.1.1, page 255]:

the minimization problem is „[...] a function f which depends on one or more independent variables $x_1, x_2, ..., x_i$ [...]“ for which the corresponding variables have to be selected in such a way that the function f takes a minimal value. For minimal values of f the following holds:

$$\frac{\partial f}{\partial x_i} = 0, \quad \frac{\partial^2 f}{\partial x_i^2} > 0 \tag{3.1}$$

[19], meaning that the first derivative of f equals 0 and only positive second derivatives exist. The energy being a function of the coordinates of the systems means that a change within the structure – a movement of the coordinates – results most likely in a change of the potential energy. Such a movement could be only a single bond rotation or a joint motion of a number of atoms; the accordingly increase or decrease of the energy as well as the shift's intensity depends on how much change occurred in the coordinates. The potential energy can be seen as a so-called *potential energy surface*, with the energy depending on the geometry of the system, for instance bond length, angles or bond rotations. With every change within the atoms' coordinates the energy function moves on the surface. A graphical representation of this *potential energy surface* is only possible for very simple cases where the energy function is just based on one or two parameters. A simple example, where the potential energy is a two-dimensional function depending on dihedral angles of the structure, is shown in Figure 3.1.

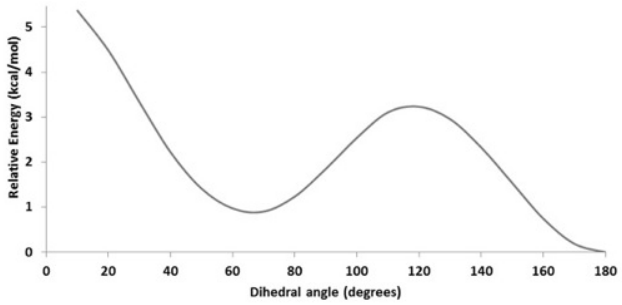

Figure 3.1: Example of the *potential energy surface* for butane depending on dihedral angles (Source: [24]).

In a mathematical point of view, those points of the surface, where the first derivative of the energy function equals zero with respect to the set of coordinates, are important for the computation of the energy minimization. These points are defined as stationary points with zero forces on all atoms. Stationary points can

be for instance minimal points of the potential energy function. A system has a minimum energy if all atoms are in a stable state. If there is a change within the coordinates and the system pulls away from a stable system, the energy increases leaving the minimum point. Furthermore, there exist so-called saddle points on the surface, which are the highest points between minimums. On a *potential energy surface* there exist different kinds of minimums. Energy minimums are often local, meaning that in their environment they do not present the lowest energy and the most stable conformation of the system. In close proximity to this minimal point, separated by some maximums and saddle points in between, there is a lower minimum on the surface, a so-called *local energy minimum*. This has to be considered when applying an algorithm for energy minimization. Besides those *local energy minimums*, there is one lowest energy minimum on the overall surface, or in a certain considered area, that is called the *global energy minimum*.

In a mathematical description, stationary points are defined as those points where the first derivative of the function with respect to the atom's coordinates is zero. Here, as was already discussed in Section 2.2, the importance of the decision of a best force field is made clear: a force field, the set of parameters describing a system, is selected in such a way that the first derivative of the energy with respect to the system's atoms can be calculated. See Figure 3.2 for a more detailed representation of a *potential energy surface* with minimums, maximums and saddle points.

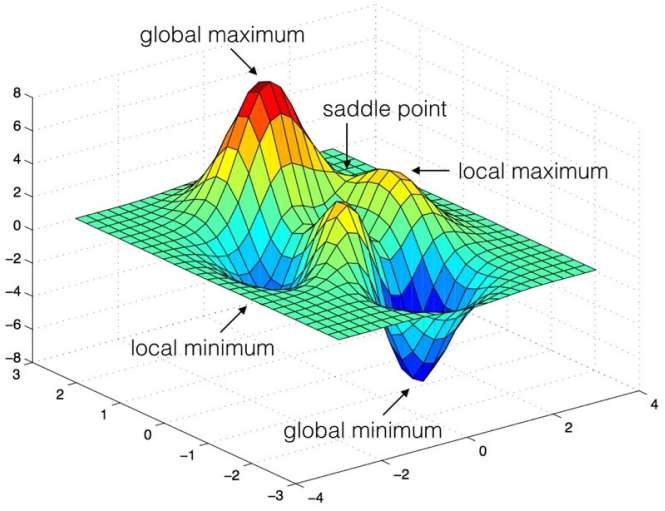

Figure 3.2: General example of the *potential energy surface* with minimums, maximums and saddle point (depicted according to [25, Figure 2]).

When choosing a minimization algorithm some crucial points need to be considered, for instance the size of the underlying system, the form of the energy function, but also storage and computational requirements and the robustness of the method. With all these factors taken into account, an energy minimum of the molecule can be computed quickly and with as few as possible resources. A very important differentiation between these minimization algorithms is how they move on the *potential energy surface* to find the energy minimum. Minimization algorithms can perform the search for the minimum downhill on the *potential energy surface*. Starting at a given initial point, the algorithm then searches for the nearest minimum, going down on the energy surface from this point (see Figure 3.3).

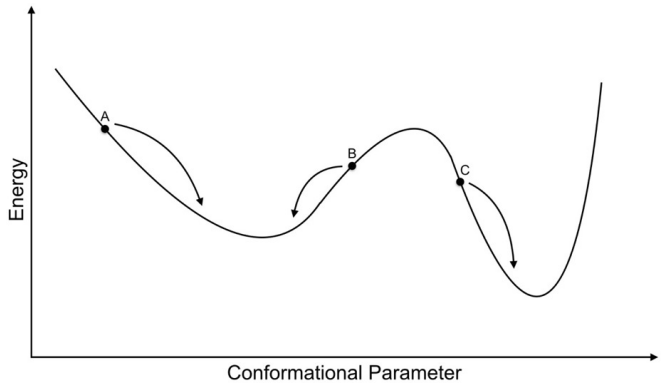

Figure 3.3: Downhill-search on a one-dimensional energy surface (depicted according to [19, Chapter 5.1.1, page 257]).

With the use of the downhill method, only a local minimum can be detected, possibly not the lowest local minimum and it is more unlikely to detect the *global energy minimum*. To assure a wider sampling of the *potential energy surface*, algorithms use many different starting points, from which they start the energy minimization concurrently, as outlined in Figure 3.3 with starting points A, B and C. Algorithms can also use the so-called uphill method to find minimums that are not the closest, but lower than those in proximity to the starting point. But these algorithms, too, are not assured to find the global minimum in any event when starting the minimization process from random initial points.

It is also important to consider the structure of the *potential energy surface*, when searching for an energy minimum, which corresponds to a conformation of the structure with very low energy. There might be a narrow minimum with low energy (a *global energy minimum*) that is very little populated, compared to a much wider and higher point (a *local energy minimum*), that represents a structure that is much more likely. This means that the biological structure is very unlikely to

change into the conformation of the *global energy minimum* but is present more often in the conformation of the local minimum. Therefore, the low-energy conformation of the global minimum might not be a suitable representation of a biological system and can lead to distorted or altered results when performing further calculations of the system.

For the calculation of the energy minimum, and especially to identify the *global energy minimum*, there exist a variety of algorithms that sample the *potential energy surface* in different ways to find a minimum. The minimization algorithms can be classified into different groups: non-derivative minimization methods, first-order minimization methods and second-order minimization methods. The first group, derivative-free minimization algorithms, such as the simplex method, Powell's conjugate direction method, or simulated annealing, are in particular applied to energy functions that are not differentiable. They require generally more steps to find a minimum on the *potential energy surface* than derivative methods. In contrast to this lies the technique of using the derivatives of the energy function, that is adopted in many of the most common minimization methods. With the use of derivatives, a more efficient way to identify the minimums is given since more information about the *potential energy surface* is obtained. Through the first derivative of the energy (the gradient), the direction, in which the energy minimum lies, is defined. With this information, the position of each atom of the system can be changed with regard to the force (force = minus the gradient), influencing to induce a lowering of the energy. The potential energy function $\mathcal{V}$ of a system, represented as set of coordinates x, can be described with the Taylor series expansion

$$\mathcal{V}(x) = \mathcal{V}(x_k) + (x - x_k) \cdot \mathcal{V}'(x_k) + (x - x_k)^2 \cdot \mathcal{V}''(x_k)/2 + ... \tag{3.2}$$

with x_k representing a molecular configuration of the system at time k [19, Chapter 5.3]. But since energy functions of molecular modeling usually are not quadratic, the Taylor series expansion is only an approximation [19], demonstrating that the process of energy minimization has to be specified thoroughly. A method that works well in proximity to a minimum may fail further away, as its approximation is poor. A good way to circumvent such problems is initially applying a robust method and accepting inefficiency, and, once closer to the minimum, continuing with a more efficient and less robust method.

First-order derivative minimization methods are for instance the *steepest descent* or *conjugate gradient* method. Those methods start at an initial and user defined configuration of the system (represented by vector x_1). Then any configuration x_k is slowly changed to reach a minimum point eventually, with input x_{k-1} for step k

obtained from the preceding step $k-1$.

Steepest Descent Method The movement's direction on the *potential energy surface* of this method is parallel to the net force. The direction for a system with $3N$ coordinates can be defined as:

$$s_k = \frac{-g_k}{|g_k|} \tag{3.3}$$

with g_k being the gradient at point k [19]. With the use of the line search method, the minimum of the potential function can be searched along the direction s_k. Briefly summarized, this technique limits a minimum on a straight line by picking 3 points on it of which the two outer points have a higher energy then the middle point. The space between the points is reduced stepwise, limiting the minimum to a smaller area. The range of a step along the direction s_k can therefore be chosen arbitrarily. With this arbitrary step approach, each step $k+1$ is a move of the coordinates x_k along direction s_k with step size λ_k (a prescribed default value in many *steepest descent* algorithms) and the new molecular configuration is defined as the following:

$$x_{k+1} = x_k + \lambda_k s_k \tag{3.4}$$

[19, chapter 5.4]. For every iteration k of the process, it is monitored if the step concludes in a lower energy level. If so, the step size λ_{k+1} is increased by a factor c_λ (e.g. 1.2, [19]). This is continued until a step results in a rise of the energy, because it is assumed that a energy minimum was exceeded. At this step, the factor c_λ is adjusted (e.g. 0.5, [19]) to reduce the step size λ to approach the energy minimum that has just been overstepped.

The constitution of the *potential energy surface* influences the step size: large step sizes work for a flat surface, whereto uneven surfaces require smaller step sizes. Compared to the line search approach, the arbitrary step method may need more steps to find a minimum, but as it often calls for less evaluations of the functions it has lower computational costs than the line search method.

In the *steepest descent* method, the direction of the gradient is derived from the largest atomic forces. This makes the method well suited for applications to an initial configuration with a high energy level. *Steepest descent* is a robust method applicable to systems distant from an energy minimum. However, a major disadvantage of this method is that it needs to conduct many small steps when sampling a narrow region of the energy surface. Since the *steepest descent* algorithm performs right-angled turns after each time step, it is – depending to the underlying

system – not the most direct and easiest way to reach the energy minimum.

Conjugate Gradient Method In comparison to the *steepest descent*, the *conjugate gradient* method has a direction vector v_k that starts the movement on the surface at point x_k. v_k is composed of the previous direction vector v_{k-1} and the gradient g at point k:

$$v_k = -g_k + \gamma_k v_{k-1} \tag{3.5}$$

with

$$\gamma_k = \frac{g_k \cdot g_k}{g_{k-1} \cdot g_{k-1}}, \tag{3.6}$$

a scaling factor for the direction [19, Chapter 5.4]. When sampling a narrow region of the energy surface, the directions generated of the *conjugate gradient* minimization do not show oscillation like the directions of the *steepest descent* method. For both algorithms, the gradients of the successive steps are orthogonal to each other. The behavior of the directions for the energy functions, however, is different: directions of the *steepest descent* algorithm are orthogonal to the direction of the prior step, whereto the *conjugate gradient* directions behave conjugate with their predecessor.

These two methods presented above are very commonly applied in molecular mechanics calculations, and can be used for minimization of small particles as well as bigger systems with thousands of atoms.

In a second-order derivative method, both, the first and the second derivative of a function are used. The second derivative holds information about the positions of a minimum or any other stationary point: it characterizes the curve of the function and can outline a point where the function changes its direction and passes a stationary point. A very simple second-order derivative method is the Newton-Rhapson method. The Newton-Rhapson method calculates a point x_{k+1} with the help of the preceding point x_k and the gradient g_k. The inversion of the Hessian matrix of the preceding point x_k is used, leading quickly to high computational costs with increasing amount of atoms in the system. This method is therefore only suitable for small systems with upto 100 atoms. Thus, variants of the Newton-Rhapson method have been developed trying to avoid this matrix calculation to reduce the computational cost.

Since it is nearly impossible to find the precise solution of the energy minimization of a system and to prevent the algorithm from continuing the search infinitely, an energy minimization algorithm receives a convergence criteria at the beginning. The convergence criteria states at which point the algorithms has reached a solution

sufficiently contiguous to the energy minimum and the calculation can be stopped. A common method is not giving a certain energy value, but a threshold for the energy difference between two steps. If the amount the energy changes between on step and its successor is less than the specified threshold, the algorithm terminates. Similarly, the conformational change can be monitored and the termination of the algorithm is induced if no significant change occurred.

3.3 Molecular Dynamics simulation

Movements of a system can be calculated applying molecular dynamics (MD) and with the use of those calculations, time averages of the system's properties can be extracted. The studied molecular system is presented in the form of a coordinate file. The set of atoms of each time step is calculated by applying Newton's equation of motion. The method of molecular dynamics is deterministic, meaning that from any current point in time, any future or past state can be predicted. With this continuity of the method, the calculation of the equation of motion is divided into a sequence of short time steps. An average length of a time step lies between 1 to 10 femtoseconds. For every time step $k + 1$ of the simulation, velocities and positions of the atoms are calculated with forces acting on each atom together with the position and velocities of time step k. The MD simulation creates a trajectory containing the dynamic change of the variables describing the system over a certain amount of time. A typical length of such a trajectory is 100 000 steps for a simulation of 100 picoseconds with a time step size of 1 femtosecond. Hence, a molecular dynamics calculation output provide properties of the underlying system depending on time, in contrast to other methods such as Monte Carlo simulations, in which no temporal connection exists between consecutive steps [19].

The process of a molecular dynamics simulation is divided into two calculations. First, the data is equilibrated (Section 3.3.1), followed by a computation that is responsible for generating the data that can be used for establishing the binding behavior of the system by analyzing its energies.

Potentials To perform a molecular dynamics simulation, a functional form for the intermolecular potential $\mathcal{U}(r^N)$ has to be selected. Algorithms used for molecular dynamics simulations can be classified into two groups: the first uses the hard-sphere potential, a potential that was used in the first ever performed MD simulation, and the second group uses soft-sphere potentials. In the first group, the intermolecular forces are discontinuous functions of the particles' distances. Particles move with constant velocity on straight lines. In hard-sphere models it is assumed that the particles have hard bodies, meaning that a collision occurs when

the distance r between two particles with positions r_1, r_2 is less or equal the sphere diameter. Thus, force are only then exerted when collision between particles takes place:

$$\mathcal{U}(r) = \begin{cases} \infty, & r \leq \sigma \\ 0, & r > \sigma \end{cases} \tag{3.7}$$

with distance r defined as $|r_1 - r_2|$ and σ the sphere's diameter [26, Chapter 3]. For the soft-sphere model of the intermolecular potential, Equation 3.7 looks the following:

$$\mathcal{U}(r) = \begin{cases} \epsilon \left(\frac{\sigma}{r}\right)^n, & r \leq \sigma \\ 0, & r > \sigma \end{cases} \tag{3.8}$$

with ϵ denoting the interaction strength and n defining the different potentials: $n = \infty$ leads to the hard-sphere model (eq. 3.7) and $n = 12$ being the Lennard-Jones potential [27]. In the hard-sphere potential, as opposed to the soft-sphere model, particles do not overlap in space, which imitates natural circumstances of particles with strong repulsion at close distances.
In this study, for non-bonded interactions between atoms the Particle Mesh Ewald (PME) method is applied. The PME method uses a hard sphere model to calculate the interactions of particles and divides interactions between the particles into long-range and short-range potentials.

Periodic Boundary Conditions Steps of a molecular dynamics simulation are often performed with periodic boundary conditions. For periodic boundary conditions the original simulated system is copied and appended to all faces of the simulation box. When introducing the periodic boundary conditions, interactions not only occur between a particle and its neighbors in the same box but also with all neighboring particles in the copies of the original box. The cells adjacent to the original simulation box ensure forces on the particles from a bigger space than actually present. A two-dimensional example of a simulation cell with periodic boundary conditions is shown in Figure 3.4: eight identical replicas of the cubic simulation box are surrounding it. Transferring this example to a three-dimensional space would mean that the original box is enclosed by 26 cells. Coordinates of the particles in the adjacent cells are calculated through adequate addition or subtraction of the box size. If an atom or particle leaves the box and enters a adjacent cell, it is also reentering the original box from the other side, since all cells show the same content and behavior. Thus, throughout the simulation each box keeps its particle content stable. There exist different shapes of simulation cells: the cube, the hexagonal prism, the truncated octahedron, the rhombic dodecahedron and the elongated dodecahedron. A requirement these shapes need to fulfill to be

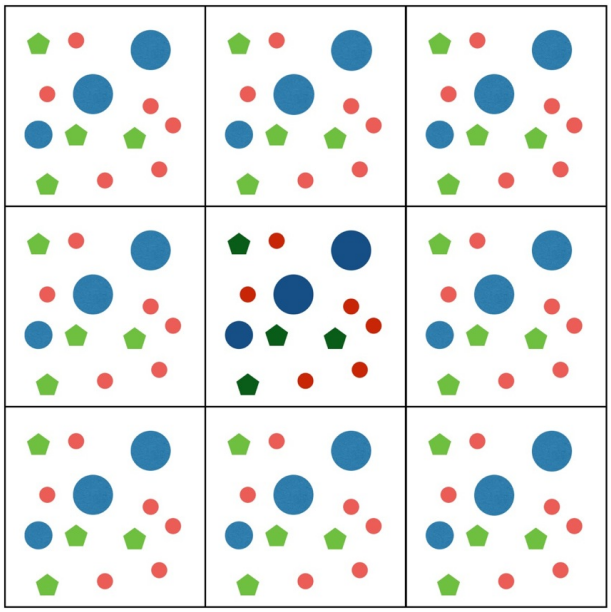

Figure 3.4: Two dimensional example of periodic boundary conditions, actual simulation box in the center in darker colors.

suitable as a simulation box, is that all space needs to be filled when applying the periodic boundary conditions and attaching duplicates of the box onto its faces. Furthermore, the shape of a simulation box should be chosen with consideration to the appearance of the system under investigation, to ensure adequate room for the molecules, but at the same time the smallest possible space to keep computational cost and storage at a minimum. The size can only be reduced to a smaller size as long as no interaction between the molecule and itself in a neighboring box occurs when applying periodic boundary conditions.
A disadvantage of the application of periodic boundary conditions is the fact, that no movement bigger than the box size can be achieved. Thus, as the computational effort benefits from a small environment with a low amount of atoms, it disadvantages when simulating system with wide range interactions and a lot of particle movement due to the necessity of a bigger simulation box.

3.3.1 Equilibration

The equilibration step of a computer simulation is performed on a system to prepare an initial conformation with an appropriate geometry and solvent orientation for the following production run. Conditions and a conformation of the system arbitrarily achieved prior to the simulation might be imprecise due to false or unfounded decisions and need to be improved. During equilibration, the system is

relaxed, hence this step is also called relaxation phase. The equilibration is carried out until relevant properties of the system are ensured to have reached a stable condition. Such properties are structural and thermodynamic features, including temperature, energies and pressure. In a starting conformation of a system consisting of a macromolecule and a solvent, the solvent could for instance be presented as a solid lattice and needs to be reduced into a liquid state before conducting the production MD run. Solvent and ions of the underlying system need to be set into a reasonable orientation around the solute within the simulation box. To conduct the molecular dynamics calculation and prevent the system from a possible collapse during the simulation, the solvent needs to be brought to a desired temperature, after which pressure can be applied to ensure suitable density of the system.

Equilibrium of a system is reached if at this point the net force f of the system is zero. The force f is defined as

$$f = -\left(\frac{dV}{dx}\right) \tag{3.9}$$

with potential energy V at position x of the system [28, Chapter 2]. The system tends to move towards and remain at a point of equilibrium, as the potential energy, a function of the degrees of freedom, can reach a minimum at this point. Different states of equilibrium can be defined: stable, metastable, unstable, and neutral equilibrium states. An equilibrium is stable if the potential energy has reached a minimum value of the system. Metastable means, that the potential is at a local minimum, but another minimum exists in proximity with a lower point. The equilibrium state is therefore unstable concerning larger movements. An unstable state of equilibrium is present if the potential energy is at a maximum value and an equilibrium is neutral at a point where the *potential energy surface* is flat [28].

The duration of the phase of relaxation is affected by the initial state of the system: the closer the conditions are to equilibrium at the beginning of the equilibration, the quicker it can be reached. Respectively, if an initial conformation and set of conditions of the present system is far from its equilibrium state, the duration of the relaxation phase increases.

Position Restraints The equilibration step is performed with the use of position restrains. This means, that on a set of atoms of the investigated structure (e.g. a protein or other macromolecule) a position restraining force is imposed. A common set of atoms could be for instance all heavy atoms of a system, meaning all atoms except hydrogen. Movements of the atoms can only be made if a significant

force was overcome. Thus, with these position restraints on the molecule of interest, no severe structural changes are caused during the equilibration of the solvent.

Ensembles The stage of equilibration is often divided into more then one steps: calculations can be conducted under different ensembles. This means, different compositions of energy, pressure, temperature, and volume are held constant throughout the calculation. In a traditional molecular dynamics simulation, the so-called microcanonical ensemble is used. The microcanonical ensemble (NVE) operates, besides having a constant number of particles N, at constant volume (V) and constant total energy (E). An extension of the microcanonical ensemble, the NVE-P ensemble, also keeps the pressure (P) at a constant level. MD simulations can also be carried out with the use of other ensembles, such as the canonical and the isobaric-isothermal ensembles. When using the canonical (NVT) ensemble, volume (V) and temperature (T) are held constant and the system's total energies can change. Simulations should be conducted at a constant temperature if the objective of this comparison is how a system behaves under different determined temperatures. Furthermore, if the conformational space is searched using the simulated annealing algorithm, the temperature is gradually reduced but kept stable between those individual steps. Contrary to this, the isobaric-isothermal (NPT) ensemble holds pressure (P) and temperature (T) at a constant level. By studying a system using the isobaric-isothermal ensemble, phase transitions caused by pressure can be observed. These circumstances are the ones most similar to the conditions present in experimental measurements and some new arrangements of the structure are obtained better with the NPT ensemble than with constant volume using the NVT ensemble.

For all above presented ensembles it is mandatory to keep the number of particles constant throughout the molecular dynamics calculations. This contrasts with the so-called grand canonical ensemble. A simulation of the grand canonical ensemble contains the possibility of an alteration of the particle composition at constant volume and temperature.

Equilibrium states of the system can be described with several energy functions, depending on the usage of the different ensembles. The microcanonical (NVE) ensemble is defined as the maximum entropy (S) of the system. The equilibrium state of the canonical (NVT) ensemble can be described as the minimum Helmholtz free energy (A), and the minimum Gibbs function (G) characterizes the equilibrium of the system when applying the isobaric-isothermal (NPT) ensemble [19].

3.3.2 Production MD

The last step of the simulation is called the production MD. To simplify matters, a molecular dynamics simulation can be viewed as a very simple program, containing the following steps: first, parameters concerning the simulation run are considered (size of the system, desired simulation length, size of time step, initial temperature). As a second step, the system is initialized, including the selection of a initial position and initial velocities. And finally, forces acting on the system's particles are computed, followed by the integration of Newton's equation of motion. The last two steps are the essential steps of the MD simulation. Until the desired length of simulation trajectory has not been reached, those steps are performed repetitively.

The calculation of forces of the system is the most time consuming part in almost all MD simulations. For this step, a distinct definition on how particles interact with each other, the so-called non-bonded interactions, is required. For instance, particles of a system can interact pairwise, meaning all particles included in the system interact with every other particle. The force of a particle i in a system of N particles is affected by all its $N-1$ neighbors. Another method, when periodic boundary conditions are applied, would be to evaluate distances between each particle and the nearest periodic image of the remaining particles. Here, every distance between any two particles i, j is calculated and then the nearest periodic image of j is taken to compute the force on particle i (for this, $N \times (N-1)/2$ distances need to be evaluated). Furthermore, the forces can be calculated with the use of a defined cut-off value. This means, that only distances below this given threshold contribute to the force of the particles, as solely a certain small distance between two particles i, j is considered to define i and j as interacting particles. To make sure that for the force calculation of a particle no periodic images of itself or more than one copy of any particle are take into account, the chosen cut-off should be a value smaller than half the box size.

As already mentioned above, this run is the construction of a trajectory containing consecutive configurations of the system. This construction is performed with the integration of Newton's law of motion, which are defined as the following:

1. Unless a force appears, an object can move at a straight, unaffected direction with constant velocity.
2. $F = m \cdot a$, with F the force of a particle, m the mass of the object and a the object's acceleration.
3. Any reaction consists of two opposing reactions: objects A reacts with some force F on object B $\iff$ object B has equal force on object A.

The various ensembles presented in Section 3.3.1 are also applied in this step. In general, the *NVE* ensemble is used for the computation of a molecular dynamics production run. The *NVE* ensemble is described with the Newton's second law of motion as

$$F(x) = -\nabla\mathcal{V}(x) = m \cdot \dot{V}(t), \quad V(t) = \dot{x}(t) \tag{3.10}$$

[29, 26]. The negative gradient of the potential energy function $\mathcal{V}$ is equal to the force F. For a distinct particle i with mass m_i and set of coordinates x_i, the motion of this particle is induced with force F_{x_i} and the corresponding differential equation related to Newton's second law can be described by the following:

$$\frac{d^2x_i}{dt^2} = \frac{F_{x_i}}{m_i} \tag{3.11}$$

[19, Chapter 7.1]. For each of the time steps, as determined prior to the calculation, the above presented equation of motion, including particle positions x and velocity V, is integrated. To determine the force F in each time step, methods such as the Verlet algorithms can be applied. The Verlet method is a simple and effective algorithm to develop a time evolution of particle position x and velocity V, the so-called trajectory. The Verlet algorithm, as well as others for the integration of motion, presume that through Taylor series expansion particle positions and other properties (such as velocities and accelerations) can be approximated. To calculate the positions of the particles x and accelerations a at a new time step $t + \delta t$, with δ being the size of a time step, the method of Verlet uses the positions and accelerations from the current and the previous steps, t and $t - \delta t$. The position of particles at time $t + \delta t$, the sum of positions at time t and $t - \delta t$, is defined as

$$x(t + \delta t) = 2x(t) - x(t - \delta t) + \delta t^2 a(t) \tag{3.12}$$

(for more details on how equation 3.12 is derived, see [19, Chapter 7.3, pp. 355-358]). The Verlet integrator does not use the velocities of the particles for the calculation of the new positions, but they can be derived from the trajectory:

$$V(t) = \frac{x(t + \delta t) - x(t - \delta t)}{2\delta t} + \delta t^2 a(t) \tag{3.13}$$

[7, chapter 4]. This is a estimation of the velocity with accuracy of order δt^2. With the new positions, the next step can be initiated: current dynamic properties, like the current potential energy, the total energy and the current temperature can be computed at this point and stored. Next, the calculation of the particle position of the subsequent step $(t + 2 \cdot \delta t)$ is performed analogously as the one before. The procedure is continued until the preliminarily defined amount of time steps have been executed and the desired trajectory size is obtained.

Another algorithm that can be applied for the integration of Newton's equation is for instance the leap-frog algorithm, an algorithm similar to the Verlet method. The leap-frog method also takes the velocities of the particles into account when computing their positions. For the calculation of the positions at time $t + \delta t$ the method uses the positions of the previous time step t, equal to the Verlet algorithm, and the velocities at half-integer time steps $V(t + \delta t)$ and $V(t - \delta t)$. One main disadvantage of the leap-frog method is that positions and velocities are not computed at the same point in time and therefore kinetic energies (derived from velocities at half-integer time steps) and potential energies (derived from the particles at integer time steps) are also not obtained from equal points in time. Thus, the total energy of the leap-frog method can not be calculated directly [19, Chapter 7].

3.4 Process of the MD simulation in this study

A general molecular dynamics simulation consists of the above presented steps (sections 3.2, 3.3.1, and 3.3.2). In this study, several different variants of these steps were performed. First, a vacuum run was conducted to create an appropriate conformation of the built core multishell nanocarrier. For this run only the polyglycerol was used and it consisted of an energy minimization and a subsequent production MD calculation. A common approach to find an initial configuration of a system that can be used as starting point of the simulation is to use a result from a previously conducted computation, such as a simulation of the pure molecule. Therefore, the output trajectory of the vacuum production MD was used to find a suitable conformation as initial configuration for the succeeding run. The system used in the second computation, starting again with an energy minimization, followed by equilibration of the system and by a final production MD, consisted in addition to the now relaxed structure of the polyglycerol also of solvent molecules and the drug dexamethasone. The equilibration of this run through consisted of two individual runs: first, a calculation with the NVT ensemble was performed, after which the NPT ensemble was applied in a second equilibration. The NVT equilibration was performed with velocity rescaling temperature coupling, similar to the Berendsen coupling thermostat. The second equilibration with NPT ensemble used the same temperature properties and Parinello-Rahman pressure coupling. This second run through of computations was performed to find an adequate binding pocket for the dexamethasone inside the nanocarrier for the subsequent third round of computations. Initially, dexamethasone was positioned outside of the polyglycerol surrounded by solvent and was then pulled into the nanocarrier using the pull code included in the Gromacs package during the production MD (see

Gromacs manual[30], Topic 6.3 for detailed instructions). The pull code requires a predefined vector to use as pulling direction for dexamethasone. This production MD was again carried out with no pressure coupling and velocity rescaling for temperature coupling. The chosen step size was 0.002 for a duration of 200 000 steps. After this production run applying the pull code, an adequate conformation for the complex consisting of dexamethasone and polyglycerol could be extracted from the trajectory as an input structure for the next step. The final run through was performed for the actual calculation of the energies of the system consisting of a drug-loaded nanocarrier. Here again, the simulation was performed with solvent and proceeded the same way as the runs before: an energy minimization was performed as initial calculation to receive an adequate energy configuration of the underlying system. Afterwards, the equilibrium of the system was calculated twice with two different ensembles (NVT and NPT) and finally, a last molecular dynamics production computation was conducted. The length of the final production run was 2 nanoseconds with 1,000,000 steps and step size 0.002. A graphical representation of this procedure is obtained in Figure 3.5.

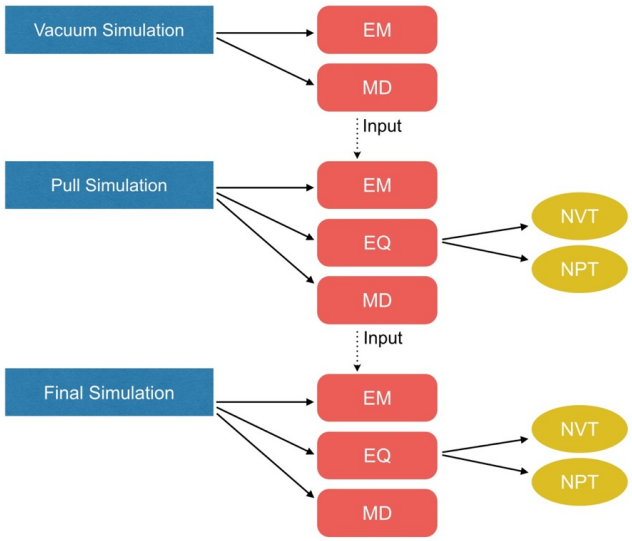

Figure 3.5: Process of the conducted simulations of this study.

When conducting a MD simulation with a solvent surrounding the system under investigation, it has to be decided what type of solvent should be used prior to the simulation. There is to choose between explicit and implicit solvent. Whilst explicit solvent results in more expensive computational costs as the implicit models, it simultaneously provides more information on how a solvent influences the solute

throughout the simulation. The benefit from including granularity and viscosity of the explicit model into the calculation of the system is essential for the defining properties such as kinetics. For the calculation of the implicit solvent on the other hand, a mean-field approach is sufficient. A very common choice of solvent surrounding the system under investigation is water, as it provides natural-like cell conditions for proteins or DNA. The water model used in all computations of this study, except the ones conducted in vacuum, was the TIP4P-Ew model. This model is a so-called 4-site model, a model having four interaction sites. One for each of the three atoms of the water molecule and an additional one close to the oxygen atom, fitted with a negative charge. This fourth interaction site leads to an improvement of the electrostatic distribution around the molecule.

For the molecular dynamics calculations in this study, a leap-frog integrator (*md* integrator in Gromacs) was used for the integration of the equation of motion.

The above described process of the simulation was carried out on two systems: the first containing the polgylcerol complexed with the drug dexamethasone, the second consisting of the same polyglycerol but in complex with dexamethasone and a spin probe attached to it. Furthermore both drugs were additionally simulated unbound, meaning only in a solvent filled simulation box of the same size. This was necessary to obtain different simulation data for the comparison of the behavior of dexamethasone and dexamethasone expanded with a spin probe. For both systems, the pull calculation was performed, but even as they were performed with the same pull vector, those differing structures resulted in different binding sites within the polymer. To provide suitable results for a subsequent comparison of the two systems, one of the generated nanocarriers including a novel binding pocket was chosen to serve as the complexing structure for the drug and its spin probe attached derivative. This means that both, dexamethasone and dexamethasone with attached spin marker, were placed at the same position inside the carrier for the performance of the final run through of the simulation.

For detailed information about the exact used parameters of the setting files for the presented steps, see Appendix B.1 to B.4.

3.5 Free energy estimation

Subsequently to the steps of the molecular dynamics runs, different kind of energies can be extracted to analyze the data. With the use of the molecular dynamics computation, many thermodynamic properties can be calculated and extracted to

provide information about the underlying system. With this information, an energy model of the system under investigation can be determined or when experimental data is also available, a comparison of the experimental and computational values of these properties can be made to establish how precise the computational methods worked. But to analyze systems for which no experimental data is possible to obtain, computer simulations can help to provide thermodynamic properties. Using thermodynamics, a molecule's reaction can be predicted, such as future binding or partitioning events of the system's components or behavior resulting in changes of shape. The first law of thermodynamics supports the forecast of a system's behavior by conservation of energy. Conservation of energy means that the total energy E of a system is stable. E is composed of kinetic energy K and the potential energy V. This leads to

$$K + V = E = \text{constant}, \tag{3.14}$$

defined through the law of conservation [28]. Kinetic energy K describes the work a system (or an object) performs on the basis of motion; work is performed by a moving object, resulting in a decrease of the object's velocity and of its kinetic energy. The kinetic energy is defined as $K = \frac{1}{2}mv^2$, with mass m and velocity v. The potential energy V was introduced in Sections 2.2 and 3.2, and can be summarized as the work performed by a system on the basis of its position. The constant total energy is ensured by the fact that throughout a process a system's kinetic and potential energy are able of change but their sum remain the same. Changes in one property are compensated by corresponding alterations in the other value, giving the characteristic that the system is a closed system. Thermodynamics' first law is a fundamental property of nature.

Looking at the thermodynamic properties, one that is considered the most important quantity is the free energy. The free energy can be described either as the Gibbs function G, applying when the system's simulation or experiment was performed under NPT ensemble, with constant number of particles, pressure and temperature, or, when a system is studied with the use of constant particles, volume and temperature, hence the NVT ensemble, the free energy is presented as the Helmholtz function A. The production MD run in this study was obtained with the NVT ensemble, thus the free energy A of a system is defined as:

$$\Delta A = \Delta U - T\Delta S \tag{3.15}$$

with inner energy U, entropy S and Δ denoting energy differences of simulated bound and unbound systems [31]. U describes hydrophobic and hydrophilic interactions of the system's components, derived from Lennard-Jones and Coulomb

energies. T is the temperature in Kelvin the system was under throughout the experiment, or in this case, the molecular dynamics calculation. All energies are calculated as a mean of the calculated period (captured in the MD trajectory) and represent an average energy value of the system. In [32], M. Weber and K. Andrae introduce a mathematical concept for the estimation of entropy differences and reformulate Equation 3.15 as the following, to define the differential entropy using terms of thermodynamic state functions U and A:

$$\Delta S = \frac{\Delta U - \Delta A}{T}. \tag{3.16}$$

The entropy S of a system is a measure describing the molecular disorder. The second law of thermodynamics states that in an isolated system, the entropy S can not decline. Non-isolated system will have a decrease in entropy but only if linked with an equal amount of entropy increase in their surroundings. The state of maximum entropy, meaning thermodynamic equilibrium, is obviously desirable for a system.

The internal energy U of a system with states $q_i \in \Omega$ is the mean energy value relating to the state's distribution. The potential energy function $V(q)$ for a state q, $V : \Omega \to \mathbb{R}$ corresponds to the inner energy of the simulation: the inner energy difference ΔU for two states $q_1, q_2 \in \Omega$ of the system can be defined as the difference of the mean of the potential energy V at those states:

$$\begin{aligned} \Delta U &= \langle V_2 \rangle - \langle V_1 \rangle \\ &= \int_{\Omega_2} V_2(q)p(q)dq - \int_{\Omega_1} V_1(q)p(q)dq \end{aligned} \tag{3.17}$$

with:

$$p(q) = \frac{exp(-\beta V_i(q))}{\int_{\Omega_i} exp(-\beta V_i(\bar{q}))d\bar{q}} \quad \text{for } i \in \{1, 2\} \tag{3.18}$$

[32]. A molecular system transforms from one conformation to another over a period of time, accompanied by changes in energies and other properties. Those different states of the molecule are reached with different probability. Equation 3.18 calculates the probability density $p(q)$ of a state $q \in \Omega$ depending on the potential energy function $V(q)$.

The free energy A of a system's state q is defined as

$$A := -\beta^{-1} \ln \left(\int_{\Omega} exp(-\beta V(q))dq \right) \tag{3.19}$$

[32]. Thus, the difference of free energy ΔA is derived from Equation 3.19 as

$$\begin{aligned}\Delta A &= -\beta^{-1} \ln \left(\frac{\int_{\Omega_2} exp(-\beta V_2(q))dq}{\int_{\Omega_1} exp(-\beta V_1(q))dq} \right) \\ &\approx -\beta^{-1} \ln \left(\frac{U_{V_1}(q_1)}{U_{V_2}(q_2)} \right) + V_2(q_2) - V_1(q_1)\end{aligned} \tag{3.20}$$

[32]. With the internal energy U (Equation 3.17) and Helmholtz free energy A (Equation 3.20) the entropy S of the system is established as

$$\Delta S \approx \frac{[\langle V_2 \rangle - V_2(q_2)] - [\langle V_1 \rangle - V_1(q_1)]}{T} + k \ln \left(\frac{U_{V_1}(q_1)}{U_{V_2}(q_2)} \right) \tag{3.21}$$

[32]. The mean of the potential energy function ($\langle V_2 \rangle$) and the potential energy function of state q_2 ($V_2(q_2)$) in the first addend of Equation 3.21 cancel each other out for a state q_2 where the potential energy $V_2(q_2)$ is equal to the mean potential energy $\langle V_2 \rangle$, meaning state q_2 represents the mean values of potential energy (for V_1 respectively).

Binding affinity The free energy difference ΔA presented in Equation 3.19 can also be use to describe the binding affinities between two systems. For a reversible transition between two systems A_1 and A_2 – this could be for instance a protein-ligand-complex with an unbound state and a binding event – the free energy difference $\Delta A = A_2 - A_1$ states which of the systems is preferred. The system with the smaller free energy value A_i is favored ($\Delta A > 0$ for system 1 and $\Delta A < 0$ for system 2) [32].

Chapter 4

Results

4.1 Pull simulation

Aim of the production run of the second round of MD simulations, the so-called pull simulation, was to find a binding site, a suitable position, for dexamethasone within the polymer. Initially, the drug was placed in the surrounding area of the nanocarrier. This start configuration can be seen in Figure 4.1(a) and (d). In Figure 4.1(a) the core of the carrier is shown as a surface representation (yellow) and the outside shell is presented as a molecular structure of atoms and bonds (red), whereto 4.1(d) represents the polyglycerol carrier as a complete surface representation (core in yellow and outside shell in red). They also show that the polyglycerol core is surrounded almost entirely by the outside shell consisting of alkyl and mPEG branches (colored red in Figures 4.1(a-f)). Using a so-called pull vector, pointing from the center of dexamethasone towards the center of the polyglycerol carrier, dexamethasone was then pulled from its current position outside the polyglycerol along the defined pull vector into the nanocarrier. The pull vector was generated with one atom central of dexamethasone and a second atom positioned in the center of the polyglycerol, see Appendix B.4 for details. In Figure 4.1(c) and (f) the end configuration of the pull run is shown, again using the above explained two ways of representation. This final state of the complex was used as input for the subsequent simulation. Figure 4.1(b) and (e) capture the time point the drug entered the carrier: the polyglycerol changed its structure to a conformation with a pore such that there was sufficient space for the drug to move inside the carrier. The path the dexamethasone took from its initial position into an artificially formed binding pocket, causing a conformation of the carrier enclosing it, can be seen in Figure 4.2. The drug moved each time step of the simulation in the direction according to the previously defined pull vector. Starting point was dexamethasone

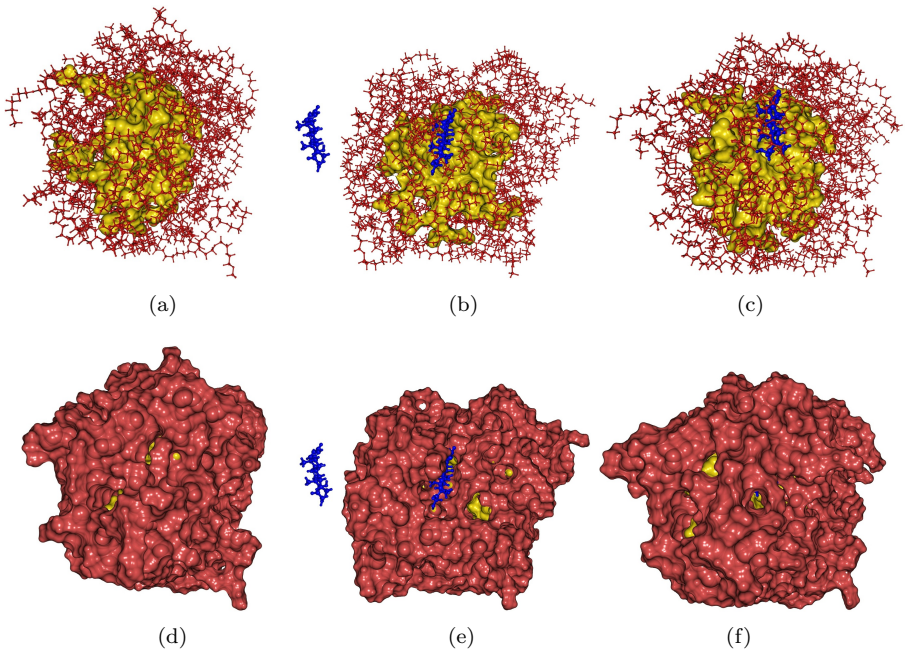

Figure 4.1: Start configuration (a,d), point of entrance into the carrier (b,e) and final configuration (c,f) of the pull-simulation. Mixture of surface and molecular representation in (a-c) and only surface presentation in (d-f).

positioned on the outside of the carrier (yellow structure in Figure 4.2) and moved then closer to the core until it reached the inner part of the carrier, the newly formed pocket (shown in Figure 4.2 in gradual color changing per time step; with dexamethasone colored yellow at its starting point and dark blue at its final position). Firstly, the drug moved closer to the surface, then the polyglycerol structure opened up and gave place to dexamethasone. Dexamethasone was thereby able to enter the nanocarrier and a change of the carrier's structure occurred afterwards. This change resulted again in a closed configuration of the nanocarrier which embraced the entered drug with its terminal branches. In 4.2 it is shown that during the process of entering the polymer, the extend to which dexamethasone moved per time step is not constant but decreases with progressing steps. Initially, when dexamethasone is not in the immediate surrounding of the carrier, the drug can take long strides per time steps in the prescribed direction. But once the drug is closer to the surface of the polymer, and even more when inside the structure, only smaller movements could be performed per time step. The size of a movement per time step performed outside the carrier was between 5 and 7.5 angstrom. Once the drug was inside the nanotransporter, moves per time step consisted only of a range between 0.1 to maximal 1 angstrom (derived from the measurements of

distances between a central point of the nanocarrier and the drug). This can be explained by the fact that far away from the polymer, dexamethasone was moving surrounded only by solvent in its proximity and was therefore only affected by forces caused through interactions with the solvent (water molecules). Once dexamethasone reached a position closer to the carrier's surface, in addition to interactions with the solvent also interactions with the polymer's structure took place. This means that much more forces influenced any possible movement of the drug. Furthermore, prior to the entry into the structure, the nanocarrier needed to give space, building some sort of pore for dexamethasone. This change of the carrier's surface structure was also induced by the interaction between the moving dexamethasone and the polyglycerol branches.

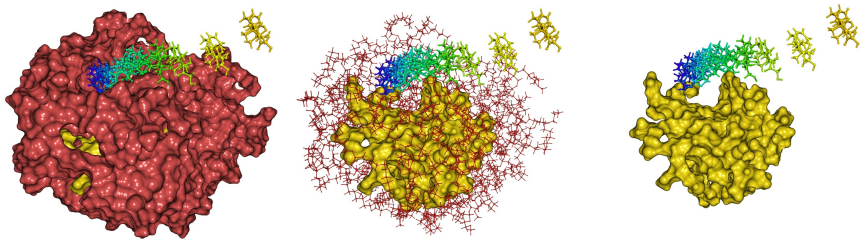

(a) (b) (c)

Figure 4.2: Dexamethasone's path into the nanocarrier as different representations. Shown is a complete surface representation (a), molecular structure representation of the outside shell and a surface representation of the surface (b), and only a surface representation of the polymer's core (c).

One might expect, that the defined pull vector would induce a path for the drug right into the polymer's center since the direction is defined as a vector from the dexamethasone's initial position to an atom at the carrier's center. But analyzing the full trajectory of the simulation revealed that throughout the whole pull calculation dexamethasone never moved inside the core. It did move very close to the glycerol core's surface, but as soon as the drug reached this point and would have had to enter the core in subsequent steps to follow the direction defined by the pull vector, the direction of movement of the dexamethasone changed and it passed by the core. This can be explained by the fact that the nanocarrier's core consists of tightly packed glycerol monomers and is therefore a very solid and dense structure. Breaking up and changing this structure would need strong forces, more than was provided by the pulling of the drug in the defined direction. Whereas the conformation of the outer shell of the carrier, consisting of long branches, could be changed as a reaction to the intruding drug. To position dexamethasone or any other loaded drug inside the dense core, mayor alterations of the structure would

be necessary to provide a suitable binding pocket for it. In Figure 4.3(a) this process is depicted in more detail for time step 103 to time step 137. The black curve represents the distance to the center, the radius of the whole molecule is displayed in red and yellow marks the core's radius. The drug was initially positioned outside the carrier (black curve at the beginning) and then passed the carrier's surface and moved inside it (black curve crossing red line). With the following steps dexamethasone approached the core but never reached its inside (black curve does move closer to the yellow line, but does not intersect it). In the final steps shown in Figure 4.3(a), the distance of dexamethasone to the center increased (black curve rises, moving away from the yellow line). In the upper left of Figure 4.3(a) a graphical representation of the radii of the polymer's core and the whole carrier is shown.

Looking at the energies throughout the simulation using the pull code, a correlation between the position of the dexamethasone and the energy can be made, demonstrated in Figure 4.3(b). Here, distances, shown in red, were measured between an atom central of dexamethasone and a point on the surface of the carrier. This surface distance was calculated as the mean of three atom positioned on the surface of the polyglycerol carrier that were identified close to the binding area. Starting outside the carrier (time step 103), the drug moved into the structure until the position for subsequent simulations was reached (time step 120). Some steps subsequent to step 120 are also depicted in this figure, capturing dexamethasone moving again away from the point it entered the surface initially. The energies calculated were interaction energies (Coulomb) of the polymer and the drug, shown in black. Initially the distance is large, meaning the drug is far away from the carrier's surface and interactions between the structures, and therefore the interaction energy, is low at this point (time step 103). With the approaching drug (decreasing distance to the surface in Graph 4.3(a)) and subsequently increasing interactions between the two structures, the energy level increases, too. A peak at time step 106 marks the point just prior to the event of entrance of the drug, conformations following this time step consisted of a carrier enclosing the drug to a certain extend. Before letting the drug enter the nanocarrier its structure changed and a kind of pore opens. This caused the distance between surface and drug to be very small, but as the distance was measured with atoms on the surface, which moved away to give space for the drug, they never reached zero. At the same time, due to changes of the structure, a rise of the interaction energy was induced. When recalling Figure 4.3(a), it is presumed that dexamethasone permeated the surface in time step 105, but this can be interpreted differently with Figure 4.3(b). Prior to the inclusion event, the nanocarrier's surface changed drastically and the structure opened to give space for the drug to enter. Dexamethasone could therefore be at a position where it was at the level of the surface but still not inside the nanocarrier.

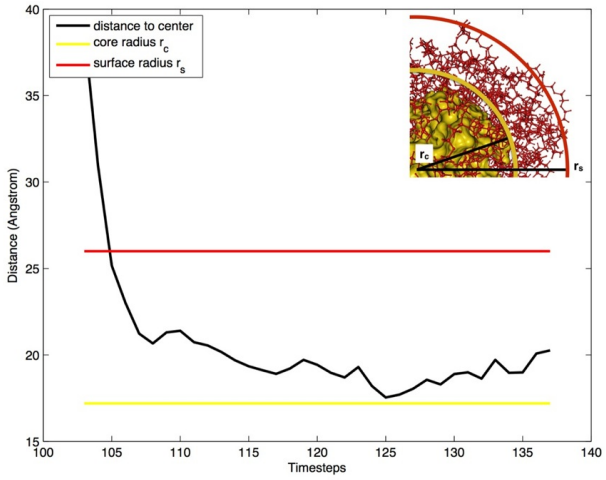

(a) Plot of distances between drug and polyglycerol's center, including radii.

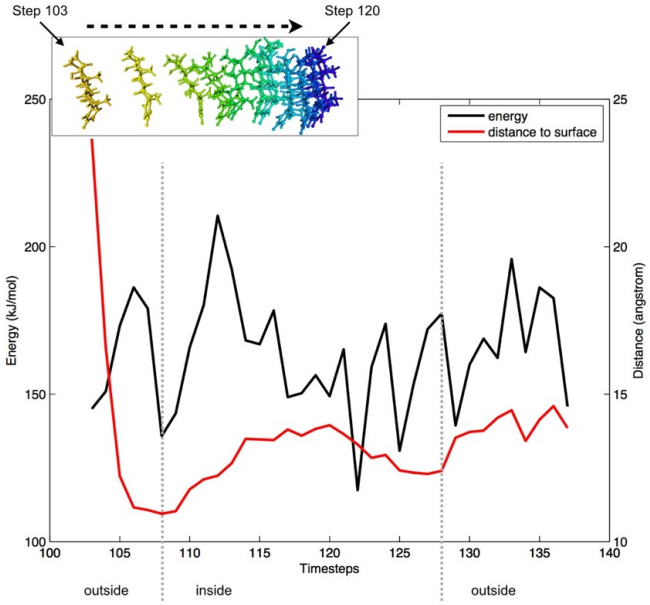

(b) Energies and distances during the pull-simulation.

Figure 4.3: Distances and energies of the complex, represented with regard to the radii of the nanocarrier.

Hence, the point of entrance into the structure is not equal to the point when the distance to the center is equal or less than the measured radius of the polyglycerol carrier. Especially, as the radius is a mean estimation of several measured values. Considering the distances and energies of the system, time step 108 can be iden-

tified as point in time when the entering of dexamethasone into the polymer was finished. At this point, the energy of the system was at a lower point compared to the preceding steps. A lot of structure modification took place previously, causing the interaction energy to be at a higher level, and providing a conformation of the nanocarrier with sufficient space for the dexamethasone to move inside. Thus, the actual event of entering did not cause a rise of the interaction energy itself but was covered in the preceding steps. Once the drug was inside the carrier (time step 110, distance to surface increasing again), the structures had to find a suitable conformation as a complex. The surface structure changed and the pore disappeared, causing the interaction energy to rise. Moving further into the carrier, meaning increasing the distance to the surface but simultaneously decreasing the distance to the center atom, the amount of drug movement per step slowed down gradually. Concurrently, the energy varied throughout these steps but was more or less balanced once the size of a time step's move became smaller. A suitable starting conformation for the subsequent simulations was found (time step 120).

Since the pull vector puts constraints on the drug, dexamethasone did not stay at a position for long. It moved again closer to the surface – decreasing distance to the surface and increasing distance to the core – and then left the carrier, but at a slightly different point of the surface, which can be seen in Figure 4.3(a): the distance to the center point increases from time step 125 on. This is also visible at time step 128 in Figure 4.3(b): the distance between dexamethasone and the surface is not as small as when entering the carrier in step 106. The event of the drug leaving the carrier leads again to an increase of the carrier's interaction energy (step 128). Occurring interactions between the drug and the polyglycerol carrier close to the surface were leading to changes in the carrier's structure and forcing it to release the drug into the solvent.

4.2 Production MD

Free energy difference Energy values of the simulated systems have been derived as presented in Section 3.5 for subsequent evaluation. The free energy difference is defined as $\Delta A = \Delta U - T\Delta S$ with ΔU being the inner energy difference, T temperature in Kelvin, and entropie difference ΔS. In this study, the inner energy U was defined as the sum of Coulomb and Lennard-Jones interaction energies derived from the interaction energies between the polymer and the solvent as well as for interactions between dexamethasone and solvent. Thus, a bound and a unbound system was simulated. The simulation concluded in the result, that the free energy difference ΔA of the system consisting of the nanocarrier and genuine

dexamethasone had a value of 16.53 kJ/mol. The free energy difference ΔA of the other system, nanocarrier in complex with the drug to which a spin probe was attached, was 23.76 kJ/mol (see Table 4.1 for detailed presentation of the single components of the energy calculation). The results of the free energy differences show that the complex with unaltered dexamethasone has a lower free energy difference than dexamethasone extended with the spin probe. The comparison of those two systems leads into the assumption that in terms of free energy, pure dexamethasone is the favored ligand in complex with a core multishell nanocarrier.

Nanocarrier system (simulation 1)	**ΔA**	**ΔU**	**$-T\Delta$S**
Dexamethasone	16.53	11.99	-4.54
Dexamethasone + spin probe	23.76	19.34	-4.42

Table 4.1: Different energy terms in kJ/mol derived from computational results of simulation 1.

Binding affinities In the following, system 1 denotes the polyglycerol carrier complexed with pure dexamethasone and system 2 describes the complex consisting of the carrier together with the spin probe attached dexamethasone. With the free energy differences of those two systems ($A_1 = \Delta A$ for system 1 and $A_2 = \Delta A$ for system 2), the binding affinity for the polyglycerol nanocarrier and its inserted drug was established as has been defined in Chapter 3.5. The difference of the free energies A_1 and A_2 of the two systems resulted in the following: $\Delta A = A_2 - A_1 = 23.76 - 16.53 = 7.23$ kJ/mol. This gives a free energy difference $\Delta A > 0$, meaning that system A_1 is preferred. Dexamethasone without the attached spin probe has therefore a higher binding affinity towards the nanocarrier than dexamethasone combined with the spin probe.
The same applies for the entropy S of the two systems 1 and 2 with S_1 describing the product of the temperature T and the entropy difference of the nanocarrier-dexamethasone system ($-T\Delta S$) and S_2, respectively, for the complex with the attached spin probe. With the entropy results S_1 and S_2 the following is given: $\Delta S = S_2 - S_1 = -4.42 - (-4.54) = 0.12$ kJ/mol. Resulting that for $\Delta S > 0$ system 1 is favored.

Additional calculations For an additional result, a second simulation was performed to yield further information about the two systems. Starting the second investigation of the complexes, a second pull calculation was conducted to find an altering binding site for the loaded drug. Results of this second round of pull calculation can be seen in Figure 4.4, where dexamethasone without (a) and with (b) spin probe are shown in blue. This position inside the nanocarrier resulting from

the pull simulation was selected as adequate binding site for the subsequently performed third round of calculations. The pull simulation, as well as the subsequent

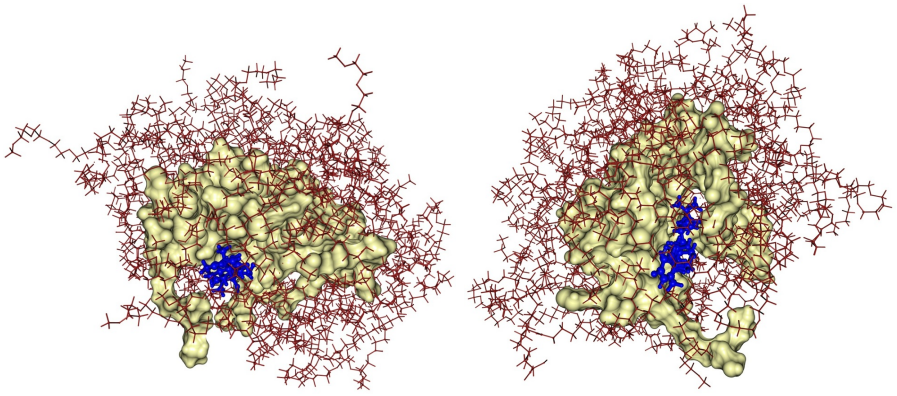

(a) (b)

Figure 4.4: Dexamethasone (a) and dexamethasone including spin probe (b) in binding pockets during the second simulation.

last run through, were again performed as presented in Chapter 3.4. Results, also calculated equally as above (Chapter 3.5), of the second calculations are presented in Table 4.2 and show a similar behavior for each of the complexes (simulation 2) as in the results presented above (simulation 1). The pull simulation concluded in a different binding pocket for the drug, but the extracted energies resulted in the same assumption as for the systems of the first performed simulation: in this binding pocket the spin probe attached to the dexamethasone showed a higher free energy difference ΔA and concurrently a lower binding affinity than the unaltered dexamethasone. Calculations of these complexes resulted even into larger differences between the energies extracted for the two systems. The binding affinity of

Nano carrier system (simulation 2)	**ΔA**	**ΔU**	**$-T\Delta$S**
Dexamethasone	-8.57	-17.16	-8.6
Dexamethasone + spin probe	32.69	26.41	-6.28

Table 4.2: Different energy terms in kJ/mol derived from computational results of simulation 2.

this second simulation was determined as $\Delta A = A_2 - A_1 = 32.69 - (-8.57) = 41.26$ kJ/mol. Resulting in $\Delta A > 0$ and giving the result that system 1 shows again a higher binding affinity towards the nanocarrier than system 2. For both binding pockets of the polyglycerol structure, pure dexamethasone is the favored structure.

The two simulations resulted in different positions of the binding site within in

the polyglycerol. A closer look at those two binding sites might give conclusions why there exists a disparity in the energy values extracted from the two runs for the same drug. Especially,s dexamethasone without the attached spin marker showed a greater deviation of the energy value between the two simulations. Figure 4.5 displays the binding sites for dexamethasone (left) and dexamethasone with spin marker (right) for the first and second simulations (top and bottom). One can see that in the first simulation (top) the loaded drug is not as far inside the polyglycerol than during the second simulation (bottom). In the second pull run, as was already seen in Figure 4.4, the two variants of dexamethasone were much deeper inside the nanocarrier, and thus, closer to the core.

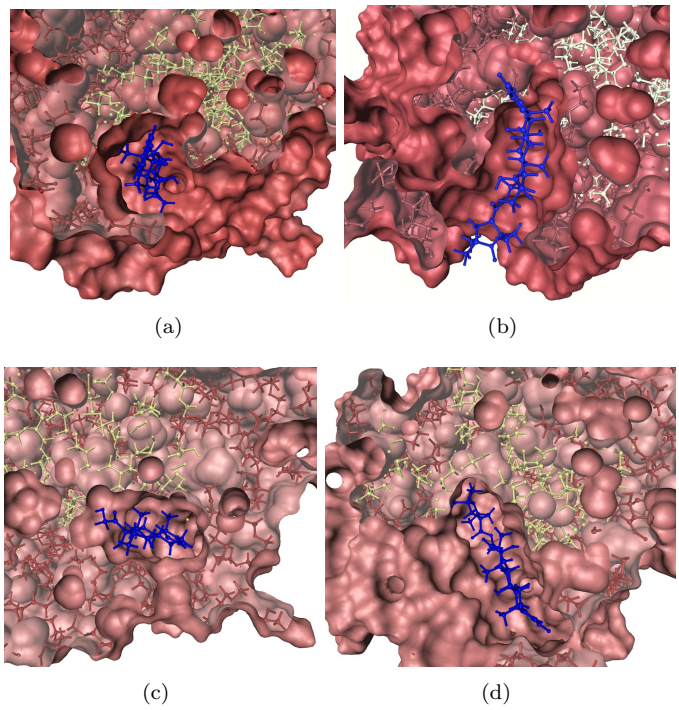

Figure 4.5: Dexamethasone (a) and dexamethasone plus spin probe (b) in their corresponding binding pockets during the first simulation and for the second simulation, (c) and (d), respectively.

Measuring the distance between the drug and the polymer's center (performed in the same way like the analysis of the first pull simulation in Section 4.1) resulted in the following: the distance between the center of the carrier and the drug was approximately twice as large for the first binding site as for the second one. This applies to both, the complex consisting of dexamethasone as well as for the polymer carrying dexamethasone plus spin marker (see Table 4.3): dexamethasone was at a range of about 18.2 angstrom during the first simulation compared to the distance

of only 9.8 angstrom for the second. The other system including the spin marker, changed from 19.8 angstrom in the first calculation to 8.3 in the second performed simulation.

Simulated system	First simulation	Second simulation
Dexamethasone	18.19Å	9.83Å
Dexamethasone + spin probe	19.81Å	8.34Å

Table 4.3: Distances in angstrom between drug and a center atom of the polymer. Measured for the two different binding sites and for each of the system.

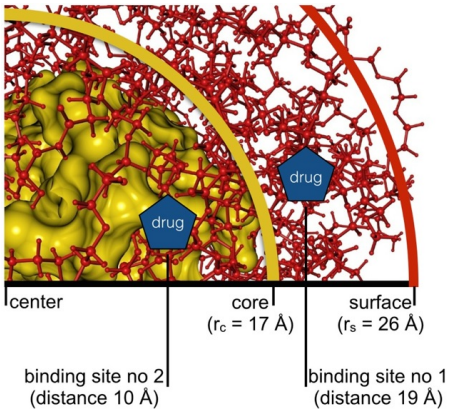

Figure 4.6: Nanocarrier with core and surface radii and binding sites.

Furthermore, the structures of the nanocarrier's core was analyzed. Differences in the structure of the polymer's core can be recognized comparing the results after the two pull simulations with their different binding sites, regardless the loaded drug. The core's structure after the first simulation is shown in Figure 4.1 and Figure 4.4 outlines the carrier's core resulting from the second simulation. A closer position of the drug to the center of the polyglycerol caused a modification of the structure. Figure 4.6 shows the various radii of the nanocarrier, the center point of the carrier, and the two different binding sites. Concerning the measured distance between the binding site of the second simulation and the center point, the drug should be positioned inside the core. The results presented above (especially Figure 4.4) show that the structure of the core was modified to present a binding site for dexamethasone and forming a pocket halfway surrounded by the core to capture the drug. Hence, the pulling of the drug did affect the core but could not enter it entirely. Nevertheless, this reshaping of the structure effects the structure of the whole nanocarrier. Prior to the pull simulations, the structures of the core were similar, as they were both using the same configuration as starting point.

Chapter 5

Discussion

The computational results presented in the previous chapter give a variety of information about the studied systems. First of all, the size of the nanocarrier had to be chosen carefully to fulfill one crucial property: it had to be big enough such that capturing the drug entirely was feasible. The structure of the nanocarrier under investigation in this study is divided into a core section and the surrounding outer shell. As it could not be specified explicitly at the beginning of the analysis in which part of the carrier dexamethasone will be positioned for drug delivery, each of these individual sections had to be of sufficient size to enclose the two variations of the drug. The nanocarrier developed in the experimental background to this study had a measured mass of 77 kDa in total. With the given specification for the amount of leaf units, a total amount of 250 individual building units could be derived. 116 of the building units belonged to the polyglycerol core (glycerol monomers) and the remaining 134 units to the outer shell, which consisted of 70% new introduced branches (94 units) and 30% conventional glycerol monomers (40 units). The parameterization of a macromolecule of such a size and composition was not feasible with the given methods of this study. For a carrier of these characteristics, being composed of the newly introduced long branches of the outer shell, the structure was packed too tight for the calculations. Due to this dense conformation, the calculations collapsed immediately. However, as has been described in [31], a reduced structure with a core of a radius of $\sim$2 nm and an outer shell consisting of the alkyl and mPEG chain of a conjoint length of $\sim$3-4 nm (both, core and shell radii prior to any MD calculation) is a suitable model of this drug delivery nanocarrier. Studying this reduced systems by applying MD simulations gave reliable and robust results concerning drug loading and the drugs' positions.

A first calculation was necessary to produce a structure that is related to the nanocarrier's natural occurrence: the branches of the outside shell coiled in such

a way that the size of the nanocarrier was reduced from 12-13 nm to 8-9 nm (dendritic core-multishell nanotransporter introduced in [31]), resulting in a reduction of 30-33.3 percent. Prior to the first calculation of this study, which was the aforementioned simulation in vacuum, the constructed carrier had an approximate diameter of 11 nm. After the vacuum simulation, the size of this structure was reduced to a diameter of 5.6 nm, a size reduction of 49 %.

The varying feasibility of MD calculations of the same nanoparticles in those two investigations can be explained by the following: in the study of Weber et al. [31], a cone shaped cutout of the structure was used for the MD simulations as a representative construction of the nanocarrier, whereas in this study the whole spherical carrier was investigated. Using the whole carrier might possibly have an impact on the calculations and will better represent real life experiments, because interactions between the drug and the nanocarrier might not only be influenced by particles in proximity to the drug but could also be influenced by parts of the carrier further away. Those interactions could not be captured in simulations of the cone shaped cutout of the nanocarrier. Furthermore, choosing a binding site in a conical model was more restricted than searching the whole nanocarrier with the use of Gromacs' pull code [30] for a position for the loaded drug. Searching the whole structure for a binding site might have led to the identification of a more natural like pocket compared to what was possible in the cone shaped carrier.
Another difference in this study, compared to the research carried out by Weber et al. [31] was the construction of the nanocarrier. In [31], the polymer assembly algorithm introduced by V. Durmaz [13] was not used, as opposed to this study. A different polymer assembly might have resulted in different levels of density and stability of the nanocarriers, consecutively leading to the varying practicability of the MD simulations, even for structures closely resembling.

Analyzing the trajectories of the pull simulation (especially shown in Figure 4.3(a) of Chapter 4.1) demonstrated that during the calculation using Gromacs' pull code [30], the drug did not enter the polyglycerol core of the nanocarrier. This could be explained by the fact that the polyglycerol structure, consisting of glycerol monomers, is a tightly packed and firm structure. A lot more force than provided by interactions between the carrier and the loaded, or „pulled“ drug, would be necessary to break up this structure and enter the core. Besides showing the feasibility of an in silico experiment, the question needs to be resolved whether breaking up the core's structure for a binding site would be practicable in real life experiments. To try entering the core with in silico experiments and to provide an altering binding site for the simulation, a second pull calculation was performed in this study. The core multishell nanocarrier used here, has no natural binding

site like many natural molecules engaged in binding events, for example proteins. Finding a binding pocket might be an adequate position, but clearly not the only possible solution. In this second pull simulation the drug was able to move inside the core to a certain extend and therefore a second binding site was found for further analysis and comparison.
Additionally, assuming that these two different positions were not only present in silico but also in real life experiments, they could be seen as an advantage as well as a drawback for the purpose of drug loading. On the one hand, the drug did not move that far inside the carrier (did not reach the core) and by that the core's structure was kept intact as well as its characterizing and stabilizing properties. Once the necessary environmental properties are obtained, drug release might be ensured more likely if the drug is closer to the carrier's surface since only the outer shell of the polymer, or even just parts of it, need to undergo a structural change. But at the same time, and what can not be investigated explicitly with the methods applied in this study, loading the drug only into an area as small and flexible as the outer shell of this nanotransporter might not be sufficient enough for keeping any drug inside the carrier as long as needed. At this point, further investigations, especially in vitro and in vivo experiments providing the appropriate surroundings of the nanocarrier medication, would be necessary to identify whether and under which conditions a drug release would be possible for dexamethasone positioned at any of these binding sites.

The results of the free energy calculation and determination of the binding affinity in Chapter 4.2 show that dexamethasone has a higher binding affinity to the nanocarrier than the structure modified with the spin probe. A smaller value of free energy difference of a system (free energy difference of its bound and unbound state) means a stronger interaction between its components [31]. This indicates that using the electron spin resonance (ESR) spectroscopy to investigate drug loading of dexamethasone into a core-multishell nanotransporter could be biased by the attachment of the required spin marker.

The results presented in this study demonstrate that different positions inside the carrier lead to different values of free energy difference ΔA for the same drug. The difference of the free energy $\Delta A = A_2 - A_1$ was calculated for two systems, free energy difference of system 1(dexamethasone) represented by A_1, and A_2 for system 2 (dexamethasone with spin probe), respectively. For the binding site closer to the core, or partly even enclosed by the core, ΔA had a higher value than for the first simulation with the binding site much closer to the surface. This greater difference between the two systems in the second simulation indicates that further inside the carrier the interactions between drug and carrier are more influenced by the spin

probe than when positioned in a binding site in the outer shell. The spin probe attached to the drug was loaded into the carrier such that the spin probe did not interact with the polyglycerol core but with the outside shell. Meaning that the interactions occurred between the spin marker's radical and the alkyl and mPEG branches leading to a weakening of the overall interactions and a lower binding affinity for the drug.

When comparing the free energy values ΔA of the same drug but in different binding sites, it gets clear that changing the position of the two binding sites induce opposite binding behavior of the two drugs. For pure dexamethasone, being positioned closer to the core results in a much smaller free energy value, meaning stronger interactions with the carrier. Dexamethasone that has been extended with the spin probe on the other hand, looses interaction strength. This second complex possesses a higher value of free energy when being bound in the binding site closer to the core. This might be due to the radical of the spin probe and its stronger influence on the interactions between the drug and the carrier when it is deeper inside the polymer structure. This means that more atoms are involved in the non-bonded interactions with the radical.
These computational outcomes might further indicate biased electron spin resonance (ESR) spectroscopy results when analyzing the drug loading of a nanocarrier. When performing ESR spectroscopy to check for a loaded drug, the attached spin marker might diminish the probability of the drug being loaded in the first place, although pure dexamethasone would have been loaded into the carrier more likely. Still, the uncertainty about the correctness of the studied binding sites has to be kept in mind when evaluating these results.

Another fact that should be acknowledged when evaluating this study, is that in real life experiments a nanocarrier is not just loaded with one unit of drug. Multiple loading is especially important and even crucial for the development of a treatment using drug delivery by nanocarriers. A high drug concentration is necessary to secure the required doses required for the treatment. But, fuller packed nanocarrier-drug complexes might behave differently than those complexes under investigation in this study that have been loaded with just one drug. This differing behavior could then be traced back to the fact that carriers loaded with more than one drug molecule possess more intermolecular interactions: the drug not only interacts with the carrier but can also be influenced by other drug molecules loaded into the carrier, especially by those in closer proximity. This might help to keep the loaded structure stable but could also induce negative impact on binding or releasing the molecules for drug delivery. Further studies concerning multiple loaded nanocarries need to be conducted to examine this issue.

Chapter 6

Conclusion

This study revealed that drug loading of a core-multishell nanotransporter with dexamethasone can not be investigated without further ado using electron spin resonance (ESR) spectroscopy. Results of the ESR spectroscopy can only be used cautiously, as attaching a spin marker to the drug might influence the drugs behavior and can lead to weakened interactions between drug and nanocarrier. Therefore, ESR spectroscopy does not necessarily capture the genuine drug's behavior inside the nanocarrier. The results revealed a higher binding affinity between pure dexamethasone and the nanocarrier compared to the spin probe attached drug. Furthermore, analyzing the two binding sites showed that different positions inside the carrier lead to interactions of differing strength. Hence, real life experiments need to be performed to analyze which position inside the carrier is more suitable for the development of a drug delivery complex. It might be possible that the formation of a binding site located to a certain degree inside the core, as it resulted in the second pull simulation, would not be feasible for a drug delivery nanocarrier in complex with dexamethasone.

Even though computational studies of a nanocarrier drug delivery system are limited to give overall results about the structures' behaviors, those computational experiments will contribute greatly to the experimental research. Studies combining computational and real world experiments, which are today still in their early stages and at the beginning of their possibilities, will have a great potential to influence future research on drug development and form novel and innovative ways of science. The combination of interdisciplinary research methods can benefit greatly from one another and lead to great innovations and success in science, especially in medical research.

Bibliography

[1] Center for Responsible Nanotechnology (CRN). (http://www.crnano.org/whatis.htm, accessed: 2015-11-29.).

[2] National Nanotechnology Initiative. (www.nano.gov, accessed: 2015-11-29).

[3] Günter Schmid, *Nanotechnology. Volume 1: Principles And Fundamentals*. WILEY-VCH Verlag GmbH & Co. KGaA, Weinheim, 2008.

[4] A. Brune, H. Ernst, A. Grundwald, W. Grünwald, H. Hoffman, H. Krug, M. R. W. Janich, P. Mayor, G. Schmid, U. Simon, V. Vogel, and D. Wyrwa, *Wissenschaftsethik und Technikfolgenabschätzung Vol. 27, Nanotechnology – Assessment and Perspectives*. Springer, Berlin, 2006.

[5] WICHLab, Jun.-Prof. Dr. Peter R. Wich, Johannes Gutenberg-Universität Mainz (http://wichlab.com/research/, accessed: 2016-02-06).

[6] R. Gupta and U. Kompella, *Nanoparticle Technology for Drug Delivery*. Drugs and the Pharmaceutical Sciences, Taylor & Francis, 2006.

[7] D. Frenkel and B. Smit, *Understanding Molecular Simulation*. Orlando, FL, USA: Academic Press, Inc., 2nd ed., 2001.

[8] M. Drescher and G. Jeschke, *EPR Spectroscopy: Applications in Chemistry and Biology*. Springer-Verlag Berlin Heidelberg, 2012.

[9] D. Hinderberger, "EPR spectroscopy in polymer science," *Top. Curr. Chem.*, no. 321, pp. 67–89, 2012.

[10] D. Peer, J. M. Karp, S. Hong, O. C. Farokhzad, R. Margalit, and R. Langer, "Nanocarriers as an emerging platform for cancer therapy," *Nat Nano*, vol. 2, no. 12, pp. 751–760, 2007.

[11] Marvin 14.7.21.0, ChemAxon. (http://www.chemaxon.com), 2014.

[12] S. KÃ$\frac{1}{4}$chler, M. R. Radowski, T. Blaschke, M. Dathe, J. Plendl, R. Haag, M. Schäfer-Korting, K. D. Kramer, "Nanoparticles for skin penetration enhancement - a comparison of a dendritic core-multishell-nanotransporter and solid lipid nanoparticles," *Eur. J. of Pharm. Biopharm.*, no. 71, pp. 243–250, 2009.

[13] V. Durmaz, "Markov model-based polymer assembly from force field-parameterized building blocks," *Journal of Computer-Aided Molecular Design*, vol. 29, pp. 225–232, 2015.

[14] S. Biswas and V. P. Torchilin, "Dendrimers for sirna delivery," *Pharmaceuticals*, vol. 6, no. 2, p. 161, 2013.

[15] D.A. Case, J.T. Berryman, R.M. Betz, D.S. Cerutti, T.E. Cheatham, III, T.A. Darden, R.E. Duke, T.J. Giese, H. Gohlke, A.W. Goetz, N. Homeyer, S. Izadi, P. Janowski, J. Kaus, A. Kovalenko, T.S. Lee, S. LeGrand, P. Li, T. Luchko, R. Luo, B. Madej, K.M. Merz, G. Monard, P. Needham, H. Nguyen, H.T. Nguyen, I. Omelyan, A. Onufriev, D.R. Roe, A. Roitberg, R. Salomon-Ferrer, C.L. Simmerling, W. Smith, J. Swails, R.C. Walker, J. Wang, R.M. Wolf, X. Wu, D.M. York and P.A. Kollman, "Amber 2015," *University of California, San Francisco*, 2015.

[16] A. W. Sousa da Silva, W. F. Vranken, "ACPYPE – AnteChamber PYthon Parser interfacE," *BMC Research Notes*, 2012.

[17] N. M. O'Boyle, M. Banck, C. A. James, C. Morley, T. Vandermeersch, and G. R. Hutchison, "Open babel: An open chemical toolbox," *J. Cheminf.*, vol. 3, 33, 2011.

[18] The Open Babel Package, version 2.3.1 (http://openbabel.org, accessed Oct 2011).

[19] A. R. Leach, *Molecular modelling: principles and applications*. Harlow, New York: Prentice Hall, 2001.

[20] http://www.meta synthesis.com/webbook/45_vsepr/VSEPR.html. (Accessed: 2016-02-09).

[21] E. Lindahl, B. Hess, and D. van der Spoel, "Gromacs 3.0: a package for molecular simulation and trajectory analysis," *Molecular modeling annual*, vol. 7, no. 8, pp. 306–317.

[22] M. J. Abraham, T. Murtola, R. Schulz, S. Páll, J. C. Smith, B. Hess, and E. Lindahl, "Gromacs: High performance molecular simulations through multi-level parallelism from laptops to supercomputers," *SoftwareX*, vol. 1–2, pp. 19–25, 2015.

[23] D. Van Der Spoel, E. Lindahl, B. Hess, G. Groenhof, A. E. Mark, and H. J. C. Berendsen, "Gromacs: Fast, flexible, and free," *Journal of Computational Chemistry*, vol. 26, no. 16, pp. 1701–1718, 2005.

[24] https://www.chem.wisc.edu/content/343esselman/conformations-of-alkanes. (Accessed: 2016-01-03).

[25] David R. Glowacki and Jeremy N. Harvey and Adrian J. Mulholland, "Taking ockham's razor to enzyme dynamics and catalysis," *Nature Chemistry*, 2012. (Accessed: 2016-03-08).

[26] J. M. Haile, *Molecular Dynamics Simulation: Elementary Methods*. New York, NY, USA: John Wiley & Sons, Inc., 1st ed., 1992.

[27] http://www.sklogwiki.org/SklogWiki/index.php/Soft_sphere_potential. (Accessed: 2016-01-14).

[28] K. A. Dill, S. Bromberg, and D. Stigter, *Molecular Driving Forces: Statistical Thermodynamics in Chemistry and Biology*. Taylor & Francis, Inc., 2003.

[29] https://en.wikipedia.org/wiki/Molecular_dynamics#Microcanonical_ensemble_.28NVE.29. (Accessed: 2016-01-12).

[30] M.J. Abraham, D. van der Spoel, E. Lindahl, B. Hess, and the GROMACS development team, "Gromacs user manual version 5.0.4," 2014. www.gromacs.org.

[31] M. Weber, C. Zoschke, A. Sedighi, E. Fleige, R. Haag, and M. Schäfer-Korting, "Free energy simulations of cargo-carrier interactions for core-multishell nanotransporters," *Journal of Nanomedicine & Nanotechnology*, vol. 5, no. 5, 2014.

[32] M. Weber and K. Andrae, "A simple method for the estimation of entropy differences," *MATCH Communications in Mathematical and in Computer Chemistry*, pp. 319–332, 2010.

Appendix A

Gromacs commands

A.1 Parameterization

Antechamber parameterization with acpype was conducted using

```
acpype -i pdb file.pdb -o pdb file.pdb
```

[16].

For the parameterization with pdb2gmx (Gromacs) the following command was called:

```
pdb2gmx -ff amber99sb -f polymer.pdb -o polymer-output.pdb -p polymer-output.top -ignh
```

resulting in coordinate and topology output files of the polymer [21, 22, 23].

Appendix B

Settings

B.1 NVT Equilibration

Parameter settings for equilibration with Gromacs (mdp file format).

```
define                  = -DPOSRES ; position restrain the protein
; Run parameters
integrator              = md
nsteps                  = 500000
dt                      = 0.002
; Output control
nstxout                 = 500
nstvout                 = 500
nstenergy               = 500
nstlog                  = 500
; Bond parameters
constraint_algorithm    = lincs
constraints             = all-bonds
lincs_iter              = 1
lincs_order             = 4
; Neighborsearching
cutoff-scheme           = Verlet
ns_type                 = grid
nstlist                 = 10
rcoulomb                = 1.0
rvdw                    = 1.0
; Electrostatics
coulombtype             = PME
pme_order               = 4
fourierspacing          = 0.16
; Temperature coupling is on
tcoupl                  = V-rescale
tc-grps                 = non-water water
tau_t                   = 0.1         0.1
ref_t                   = 293 293
; Pressure coupling is off
```

```
pcoupl                  = no
; Periodic boundary conditions
pbc                     = xyz
; Dispersion correction
DispCorr                = EnerPres
; Velocity generation
gen_vel                 = yes
gen_temp                = 300
gen_seed                = -1
```

B.2 NPT Equilibration

The second round of equilibration was performed using the *NPT* ensemble meaning the calculations were executed with constant pressure. Most of the settings were the same as for the *NVT* equilibration (Appendix B.1), except some additional parameters for pressure and velocity properties.

```
; Pressure coupling is on
pcoupl                  = Parrinello-Rahman
pcoupltype              = isotropic
tau_p                   = 2.0
ref_p                   = 1.0
compressibility         = 4.5e-5
refcoord_scaling        = com
; Velocity generation
gen_vel                 = no
```

B.3 Final Simulation

Parameter settings for production run with Gromacs (mdp file format).

```
; run parameters
integrator              = md
nsteps                  = 250000
dt                      = 0.001
constraints             = none
nstcomm                 = 1
ns_type                 = grid
; cut off distances
rlist                   = 1.4
rcoulomb                = 1.4
rvdw                    = 1.4
coulombtype             = PME
; pressure and temperature coupling
Tcoupl                  = v-rescale
tau_t                   = 0.1  0.1
tc_grps                 = non-water  water
ref_t                   = 293  293
```

```
Pcoupl                  = no
Pcoupltype              = isotropic
tau_p                   = 0.5
compressibility         = 4.5e-5
ref_p                   = 1.0
; output control
nstxout                 = 500 ; write coords every ... step
xtc_grps                = Protein dex SOL
energygrps              = Protein dex SOL
nstenergy               = 500
lincs-iter              = 2
DispCorr                = EnerPres
optimize_fft            = yes
; Generate velocites is on at 300 K.
gen_vel                 =  yes
gen_temp                =  293
gen_seed                =  -1
```

B.4 Pull Simulation

The pull simulation used the same Gromacs setting file (mdp file format) as the final round of simulation (Appendix B.3) but with the following additional settings:

```
; Pull code
pull                    = constant-force
pull_geometry           = direction-periodic
pull_dim                = Y Y Y
pull_nstxout            = 500
pull_nstfout            = 500
pull_ngroups            = 1
pull_group1             = dex
pull_pbcatom1           = 0
pull_k1                 = 30
pull_vec1               = -29.126  -6.725  -12.451
```